Chapter 13

Two-Phase Pressure Drops

(Revised in 2006)

Summary: Accurate prediction of two-phase pressure drops in direct-expansion and flooded evaporators, in tube-side and shell-side condensers, and in two-phase transfer lines is of paramount importance to the design and optimization of refrigeration, air-conditioning and heat pump systems. Taking direct-expansion evaporators as an example, the optimal use of the two-phase pressure drop to obtain the maximum flow boiling heat transfer performance is one of the primary design goals. In these evaporators, typically a two-phase pressure drop equivalent to a loss of 1.4°C (2.5°F) in saturation temperature from inlet to outlet is set as the design limit. Yet, pressure drops predicted using leading methods differ by up to 100%. Putting this into perspective, if an evaporator is inaccurately designed with a two-phase pressure drop only one-half the real value, then the system efficiency will suffer accordingly from the larger than expected fall in saturation temperature and pressure through the evaporator. On the other hand, if the predicted pressure drop is too large by a factor of two, then fewer tubes of longer length could have been utilized to obtain a more compact unit. Hence, accurate prediction of two-phase pressure drops is a key aspect in the first law and second law optimization of these systems.

In this chapter, methods for predicting two-phase pressure drops for flows inside tubes (horizontal and vertical) and for flows over tube bundles (horizontal) will be presented. In addition, two-phase pressure drop data for microfin tubes and corrugated tubes will be presented and a prediction method for microfin tubes described.

13.1 Homogeneous Flow Model Applied to Intube Flow

A homogeneous fluid is a convenient concept for modeling of two-phase pressure drops; it is a pseudo-fluid that obeys the conventional design equations for single-phase fluids and is characterized by suitably averaged properties of the liquid and vapor phase. The homogeneous design approach is presented below.

The total pressure drop of a fluid is due to the variation of kinetic and potential energy of the fluid and that due to friction on the walls of the flow channel. Thus, the total pressure drop Δp_{total} is the sum of the static pressure drop (elevation head) Δp_{static}, the momentum pressure drop (acceleration) Δp_{mom}, and the frictional pressure drop Δp_{frict}:

$$\Delta p_{total} = \Delta p_{static} + \Delta p_{mom} + \Delta p_{frict} \qquad [13.1.1]$$

The static pressure drop for a homogeneous two-phase fluid is:

$$\Delta p_{static} = \rho_H \, g \, H \sin \theta \qquad [13.1.2]$$

where H is the vertical height, θ is the angle with respect to the horizontal, and the homogeneous density ρ_H is

$$\rho_H = \rho_L \, (1 - \varepsilon_H) + \rho_G \, \varepsilon_H \qquad [13.1.3]$$

and ρ_L and ρ_G are the liquid and gas (or vapor) densities, respectively. The homogeneous void fraction ε_H is determined from the quality x as

$$\varepsilon_H = \frac{1}{1+\left(\frac{u_G}{u_L}\frac{(1-x)}{x}\frac{\rho_G}{\rho_L}\right)} \qquad [13.1.4]$$

where u_G/u_L is the velocity ratio, or slip ratio (S), and is equal to 1.0 for a homogeneous flow. The momentum pressure gradient per unit length of the tube is:

$$\left(\frac{dp}{dz}\right)_{mom} = \frac{d\left(\dot{m}_{total}/\rho_H\right)}{dz} \qquad [13.1.5]$$

The most problematic term is the frictional pressure drop, which can be expressed as a function of the *two-phase friction factor* f_{tp}, and for a steady flow in a channel with a constant cross-sectional area is:

$$\Delta p_{frict} = \frac{2 f_{tp} L \dot{m}_{total}^2}{d_i \rho_{tp}} \qquad [13.1.6]$$

The friction factor may be expressed in terms of the Reynolds number by the Blasius equation:

$$f_{tp} = \frac{0.079}{Re^{0.25}} \qquad [13.1.7]$$

where the Reynolds number is

$$Re = \frac{\dot{m}_{total} d_i}{\mu_{tp}} \qquad [13.1.8]$$

The viscosity for calculating the Reynolds number can be chosen as the viscosity of the liquid phase or as a quality averaged viscosity μ_{tp}:

$$\mu_{tp} = x\,\mu_G + (1-x)\,\mu_L \qquad [13.1.9]$$

This correlation is suitable for mass velocities greater than 2000 kg/m^{2}s (1,471,584 lb/h ft^2) in the case of the frictional pressure drop calculations and for mass velocities less than 2000 kg/m^{2}s (1,471,584 lb/h ft^2) and $(\rho_L/\rho_G) < 10$ for gravitational pressure drop calculations. Generally speaking this correlation should be used at high-reduced pressures and very high mass velocities.

Example Calculation: Using the homogeneous flow pressure drop method, calculate the two-phase pressure drop for up-flow in a vertical tube of 10 mm internal diameter that is 2 m long. The flow is adiabatic, the mass flow rate is 0.02 kg/s and the vapor quality is 0.05. The fluid is R-123 at a saturation temperature of 3°C and saturation pressure of 0.37 bar, whose physical properties are: liquid density = 1518 kg/m3, vapor density = 2.60 kg/m3, liquid dynamic viscosity = 0.0005856 kg/m s, vapor dynamic viscosity = 0.0000126 kg/m s.

Solution: The homogeneous void fraction εH is determined from the quality x using Eq. 13.1.4 where uG/uL = 1:

$$\varepsilon_H = \frac{1}{1+\left(\left(\frac{u_G}{u_L}\right)\frac{(1-x)}{x}\frac{\rho_G}{\rho_L}\right)} = \frac{1}{1+\left((1)\frac{(1-0.05)}{0.05}\frac{2.60}{1518}\right)} = 0.9685$$

The homogeneous density ρH is obtained using Eq. 13.1.3:

$$\rho H = \rho L\,(1 - \varepsilon H) + \rho G\,\varepsilon H = 1518(1 - 0.9685) + 2.60(0.9685) = 50.3 \text{ kg / m3}$$

The static pressure drop for a homogeneous two-phase fluid with H = 2 m and θ = 90° is obtained using Eq. 13.1.2:

$$\Delta pstatic = \rho H\, g\, H \sin\theta = 50.3(9.81)(2)\sin 90° = 987 \text{ N / m2}$$

The momentum pressure drop is Δpmom = 0 since the vapor quality is constant from inlet to outlet. The viscosity for calculating the Reynolds number choosing the quality averaged viscosity μtp: is obtained with Eq. 13.1.9:

$$\mu tp = x\,\mu G + (1 - x)\,\mu L = 0.05(0.0000126) + (1 - 0.05)(0.0005856) = 0.000557 \text{ kg / m s}$$

The mass velocity is calculated by dividing the mass flow rate by the cross-sectional area of the tube and is 254.6 kg/m2s. The Reynolds number is then obtained with Eq. 13.1.8:

$$\text{Re} = \frac{\dot{m}_{total} d_i}{\mu_{tp}} = \frac{254.6(0.01)}{0.000557} = 4571$$

The friction factor is obtained from Eq. 13.1.7:

$$f_{tp} = \frac{0.079}{\text{Re}^{0.25}} = \frac{0.079}{4571^{0.25}} = 0.00961$$

The frictional pressure drop is then obtained with Eq. 13.1.6:

$$\Delta p_{frict} = \frac{2 f_{tp} L \dot{m}^2_{total}}{d_i \rho_{tp}} = \frac{2(0.00961)(2)(254.6^2)}{0.01(50.3)} = 4953 \text{ N / m}^2$$

Thus, the total pressure drop is obtained with Eq. 13.1.1:

$$\Delta ptotal = \Delta pstatic + \Delta pmom + \Delta pfrict = 987 + 0 + 4953 = 5940 \text{ N/m2} = 5.94 \text{ kPa (0.86psi)}$$

13.2 Separated Flow Models for Flows inside Plain Tubes

The two-phase pressure drops for flows inside tubes are the sum of three contributions: the static pressure drop Δp_{static}, the momentum pressure drop Δp_{mom} and the frictional pressure drop Δp_{frict} as:

$$\Delta p_{total} = \Delta p_{static} + \Delta p_{mom} + \Delta p_{frict} \qquad [13.2.1]$$

The static pressure drop is given by

$$\Delta p_{static} = \rho_{tp}\, g\, H \sin\theta \qquad [13.2.2]$$

For a horizontal tube, there is no change in static head, i.e. H = 0 so $\Delta p_{static} = 0$ while sinθ is equal to 1.0 for a vertical tube. The momentum pressure drop reflects the change in kinetic energy of the flow and is for the present case given by:

$$\Delta p_{mom} = \dot{m}_{total}^2 \left\{ \left[\frac{(1-x)^2}{\rho_L(1-\varepsilon)} + \frac{x^2}{\rho_G \varepsilon} \right]_{out} - \left[\frac{(1-x)^2}{\rho_L(1-\varepsilon)} + \frac{x^2}{\rho_G \varepsilon} \right]_{in} \right\} \qquad [13.2.3]$$

where $\dot{m}_{total}$ is the total mass velocity of liquid plus vapor and x is the vapor quality.

The separated flow model considers the two phases to be artificially separated into two streams, each flowing in its own pipe. The areas of the two pipes are proportional to the void fraction ε. Numerous methods are available for predicting the void fraction. It is recommended here to use the Steiner (1993) version of the drift flux model of Rouhani and Axelsson (1970):

$$\varepsilon = \frac{x}{\rho_G}\left[(1+0.12(1-x))\left(\frac{x}{\rho_G} + \frac{1-x}{\rho_L} \right) + \frac{1.18(1-x)\left[g\sigma(\rho_L - \rho_G) \right]^{0.25}}{\dot{m}_{total}^2 \rho_L^{0.5}} \right]^{-1} \qquad [13.2.4a]$$

For vertical flows, the Rouhani and Axelsson (1970) expression can be used when ε > 0.1:

$$\varepsilon = \frac{x}{\rho_G}\left[\left[1+0.2(1-x)\left(\frac{g d_i \rho_L^2}{\dot{m}_{total}^2} \right)^{1/4} \right]\left(\frac{x}{\rho_G} + \frac{1-x}{\rho_L} \right) + \frac{1.18(1-x)\left[g\sigma(\rho_L - \rho_G) \right]^{0.25}}{\dot{m}_{total} \rho_L^{0.5}} \right]^{-1} \qquad [13.2.4b]$$

The two-phase density is obtained from:

$$\rho_{tp} = \rho_L(1-\varepsilon) + \rho_G \varepsilon \qquad [13.2.4c]$$

The momentum pressure drop is calculable by input of the inlet and outlet vapor qualities. When measuring two-phase pressure drops for evaporation in horizontal tubes, for instance, the frictional pressure drop is obtainable by subtracting the momentum pressure drop from the measured total pressure drop since the static pressure drop is nil.

For an evaporating flow, the kinetic energy of the outgoing flow is larger than that of the incoming flow since the density of the vapor phase is less than that of the liquid. Hence, the momentum pressure drop results in a lower pressure at the exit than at the inlet. Instead, for a condensing flow the kinetic energy of the outgoing flow is smaller than that of the incoming flow. Hence, the momentum pressure drop results in an increase in pressure at the exit than at the inlet, i.e. a pressure recovery. For condensing flows, it is common to ignore the momentum recovery as only some of it may actually be realized in the flow and ignoring it provides some conservatism in the design.

The frictional pressure drop in two-phase flows is typically predicted using separated flow models. The first of these analyses was performed by Lockhart and Martinelli (1949) and then followed by many others. The basic equations for the separated flow model are not dependent on the particular flow configuration adopted. It is assumed that the velocities of each phase are constant, in any given cross-section, within the zone occupied by the phase. Some common methods for *intube* flow will be given below.

13.2.1 Friedel correlation

The correlation method of Friedel (1979) utilizes a two-phase multiplier:

$$\Delta p_{frict} = \Delta p_L \Phi_{fr}^2 \qquad [13.2.5]$$

where Δp_L is calculated for the liquid-phase flow as

$$\Delta p_L = 4 f_L (L/d_i) \dot{m}_{total}^2 (1/2\rho_L) \qquad [13.2.6]$$

The liquid friction factor f_L and liquid Reynolds number are obtained from

$$f = \frac{0.079}{Re^{0.25}} \qquad [13.2.7]$$

$$Re = \frac{\dot{m}_{total} d_i}{\mu} \qquad [13.2.8]$$

using the liquid dynamic viscosity μ_L. His two-phase multiplier is

$$\Phi_{fr}^2 = E + \frac{3.24FH}{Fr_H^{0.045} We_L^{0.035}} \qquad [13.2.9]$$

The dimensionless factors Fr_H, E, F and H are as follows:

$$Fr_H = \frac{\dot{m}_{total}^2}{g d_i \rho_H^2} \qquad [13.2.10]$$

$$E = (1-x)^2 + x^2 \frac{\rho_L f_G}{\rho_G f_L} \qquad [13.2.11]$$

$$F = x^{0.78}(1-x)^{0.224} \qquad [13.2.12]$$

$$H = \left(\frac{\rho_L}{\rho_G}\right)^{0.91} \left(\frac{\mu_G}{\mu_L}\right)^{0.19} \left(1 - \frac{\mu_G}{\mu_L}\right)^{0.7} \qquad [13.2.13]$$

The liquid Weber We_L is defined as:

$$We_L = \frac{\dot{m}_{total}^2 d_i}{\sigma \rho_H} \qquad [13.2.14]$$

using the following alternative definition of the homogeneous density ρ_H based on vapor quality:

$$\rho_H = \left(\frac{x}{\rho_G} + \frac{1-x}{\rho_L} \right)^{-1} \qquad [13.2.15]$$

This method is typically that recommended when the ratio of (μ_L/μ_G) is less than 1000 is applicable to vapor qualities from $0 \le x \le 1$.

13.2.2 Lockhart and Martinelli correlation

The method of Lockhart and Martinelli (1949) is the original method that predicted the two-phase frictional pressure drop based on a two-phase multiplier for the liquid-phase, or the vapor-phase, respectively, as:

$$\Delta p_{frict} = \Phi_{Ltt}^2 \Delta p_L \qquad [13.2.16]$$

$$\Delta p_{frict} = \Phi_{Gtt}^2 \Delta p_G \qquad [13.2.17]$$

where Eq. 13.2.6 is used for Δp_L with (1-x)2 applied to the mass velocity term and Δp_G is obtained from

$$\Delta p_G = 4 f_G (L/d_i) \dot{m}_{total}^2 x^2 (1/2\rho_G) \qquad [13.2.18]$$

The single-phase friction factors of the liquid f_L and the vapor f_G, are calculated using Eq. 13.2.7 with their respective physical properties. Their corresponding two-phase multipliers are

$$\Phi_{Ltt}^2 = 1 + \frac{C}{X_{tt}} + \frac{1}{X_{tt}^2}, \text{for } Re_L > 4000 \qquad [13.2.19]$$

$$\Phi_{Gtt}^2 = 1 + CX_{tt} + X_{tt}^2, \text{for } Re_L < 4000 \qquad [13.2.20]$$

where X_{tt} is the Martinelli parameter for both phases in the turbulent regimes defined as

$$X_{tt} = \left(\frac{1-x}{x} \right)^{0.9} \left(\frac{\rho_G}{\rho_L} \right)^{0.5} \left(\frac{\mu_L}{\mu_G} \right)^{0.1} \qquad [13.2.21]$$

The value of C in Eqs. 13.2.19 and 13.2.20 depends on the regimes of the liquid and vapor. The appropriate values to use are listed in Table 13.1. The correlation of Lockhart and Martinelli is applicable to the vapor quality range of $0 < x \le 1$.

Table 13.1. Values of C

Liquid	Gas	C
Turbulent	Turbulent	20
Laminar	Turbulent	12
Turbulent	Laminar	10
Laminar	Laminar	5

13.2.3 Grönnerud correlation

The method of Grönnerud (1972) was developed specifically for refrigerants and is as follows:

$$\Delta p_{frict} = \Phi_{gd}\, \Delta p_L \qquad [13.2.22]$$

and his two-phase multiplier is

$$\Phi_{gd} = 1 + \left(\frac{dp}{dz}\right)_{Fr} \left[\frac{\left(\frac{\rho_L}{\rho_G}\right)}{\left(\frac{\mu_L}{\mu_G}\right)^{0.25}} - 1 \right] \qquad [13.2.23]$$

where Eq. 13.2.6 is used for Δp_L. His frictional pressure gradient depends on the Froude number and is

$$\left(\frac{dp}{dz}\right)_{Fr} = f_{Fr}\left[x + 4\left(x^{1.8} - x^{10} f_{Fr}^{0.5}\right)\right] \qquad [13.2.24]$$

When applying this expression, if the liquid Froud number $Fr_L \geq 1$, then the friction factor $f_{Fr} = 1.0$, or if $Fr_L < 1$, then:

$$f_{Fr} = Fr_L^{0.3} + 0.0055\left(\ln\frac{1}{Fr_L}\right)^2 \qquad [13.2.25]$$

where

$$Fr_L = \frac{\dot{m}_{total}^2}{g d_i \rho_L^2} \qquad [13.2.26]$$

The correlation of Grönnerud is applicable to vapor qualities from $0 \leq x < 1$.

13.2.4 Chisholm correlation

Chisholm (1973) proposed an extensive empirical method applicable to a wide range of operating conditions. His two-phase frictional pressure drop gradient is given as

$$\left(\frac{dp}{dz}\right)_{frict} = \left(\frac{dp}{dz}\right)_{L} \Phi_{Ch}^{2} \qquad [13.2.27]$$

The frictional pressure gradients for the liquid and vapor phases are:

$$\left(\frac{dp}{dz}\right)_{L} = f_{L} \frac{2\dot{m}_{total}^{2}}{d_i \rho_L} \qquad [13.2.28]$$

$$\left(\frac{dp}{dz}\right)_{G} = f_{G} \frac{2\dot{m}_{total}^{2}}{d_i \rho_G} \qquad [13.2.29]$$

The friction factors are obtained with Eq. 13.2.7 using Eq. 13.2.8 and the respective dynamic viscosities of the liquid and the vapor for turbulent flows while for laminar flows (Re < 2000)

$$f = 16 / Re \qquad [13.2.30]$$

The flow is considered here to be fully turbulent at Re ≥ 2000 to avoid an undefined interval in his method. The parameter Y is obtained from the ratio of the frictional pressure gradients:

$$Y^2 = \frac{(dp/dz)_G}{(dp/dz)_L} \qquad [13.2.31]$$

His two-phase multiplier is then determined as:

$$\Phi_{Ch}^{2} = 1 + (Y^2 - 1)\left[Bx^{(2-n)/2}(1-x)^{(2-n)/2} + x^{2-n}\right] \qquad [13.2.32]$$

where n is the exponent from the friction factor expression of Blasius (n = 0.25). For 0 < Y < 9.5, Chisholm's parameter B is calculated as:

$$\begin{aligned} B &= \frac{55}{\dot{m}_{total}^{1/2}} && \text{for } \dot{m}_{total} \geq 1900 \text{ kg/m}^2\text{s} \\ B &= \frac{2400}{\dot{m}_{total}} && \text{for } 500 < \dot{m}_{total} < 1900 \text{ kg/m}^2\text{s} \\ B &= 4.8 && \text{for } \dot{m}_{total} < 500 \text{ kg/m}^2\text{s} \end{aligned} \qquad [13.2.33]$$

For 9.5 < Y < 28, then B is calculated as:

$$\begin{aligned} B &= \frac{520}{Y\dot{m}_{total}^{1/2}} && \text{for } \dot{m}_{total} \leq 600 \text{ kg/m}^2\text{s} \\ B &= \frac{21}{Y} && \text{for } \dot{m}_{total} > 600 \text{ kg/m}^2\text{s} \end{aligned} \qquad [13.2.34]$$

For Y > 28, then B is calculated as:

$$B = \frac{15000}{Y^2 \dot{m}_{total}^{1/2}} \qquad [13.2.35]$$

In the above expressions, to convert kg/m^{2}s to lb/h ft^2, multiply by 735.8. The correlation of Chisholm is applicable to vapor qualities from $0 \le x \le 1$.

13.2.5 Bankoff correlation

This method of Bankoff (1960) is an extension of the homogeneous model. His two-phase frictional pressure gradient is

$$\left(\frac{dp}{dz}\right)_{frict} = \left(\frac{dp}{dz}\right)_L \Phi_{Bf}^{\frac{7}{4}} \qquad [13.2.36]$$

The liquid-phase friction pressure gradient is calculated with Eq. [13.2.28] and his two-phase multiplier is

$$\Phi_{Bf} = \frac{1}{1-x}\left[1-\gamma\left(1-\frac{\rho_G}{\rho_L}\right)\right]^{\frac{3}{7}}\left[1+x\left(\frac{\rho_L}{\rho_G}-1\right)\right] \qquad [13.2.37]$$

where

$$\gamma = \frac{0.71+2.35\left(\frac{\rho_G}{\rho_L}\right)}{1+\left(\frac{1-x}{x}\right)\left(\frac{\rho_G}{\rho_L}\right)} \qquad [13.2.38]$$

This method is applicable to vapor qualities from $0 < x < 1$.

13.2.6 Chawla correlation

Chawla (1967) suggested the following method based on the vapor pressure gradient:

$$\left(\frac{dp}{dz}\right)_{frict} = \left(\frac{dp}{dz}\right)_G \Phi_{Chawla} \qquad [13.2.39]$$

The vapor-phase frictional pressure gradient is determined from Eq. 13.2.29 and the two-phase multiplier is

$$\Phi_{Chawla} = x^{1.75}\left[1+S\left(\frac{1-x}{x}\frac{\rho_G}{\rho_L}\right)\right]^{2.375} \qquad [13.2.40]$$

and his slip ratio S is:

$$S = \frac{u_G}{u_L} = \frac{1}{9.1\left[\frac{1-x}{x}\left(Re_G\, Fr_H\right)^{-0.167}\left(\frac{\rho_L}{\rho_G}\right)^{-0.9}\left(\frac{\mu_L}{\mu_G}\right)^{-0.5}\right]} \qquad [13.2.41]$$

where Fr_H is determined with Eq. 13.2.10 and Re_G is determined with Eq. 13.2.8 using the vapor viscosity. His method is for vapor qualities from $0 < x < 1$.

13.2.7 Müller-Steinhagen and Heck correlation

Müller-Steinhagen and Heck (1986) proposed a two-phase frictional pressure gradient correlation that is in essence an empirical interpolation between all liquid flow and all vapor flow:

$$\left(\frac{dp}{dz}\right)_{frict} = G(1-x)^{1/3} + Bx^3 \qquad [13.2.42]$$

where the factor G is

$$G = A + 2\,(B - A)\,x \qquad [13.2.43]$$

The factors A and B are the frictional pressure gradients for all the flow liquid $(dp/dz)_L$ and all the flow vapor $(dp/dz)_G$, obtained respectively from Eqs. 13.2.28 and 13.2.29. Tribbe and Müller-Steinhagen (2000) have shown that this method gave the best results in a comparison of competing methods to a large database that covered air-oil, air-water, water-steam and several refrigerants, applicable for $0 \le x \le 1$.

13.2.8 Comparison of above methods to more recent databases

Whalley (1980) made an extensive comparison between various published correlations, and the HTFS database (which consisted of over 25,000 data points). The recommendations he made are as follows:

- $(\mu_L/\mu_G) < 1000$ and mass velocities less than 2000 kg/m^{2}s (1,471,584 lb/h ft^2), the Friedel (1979) correlation should be used.
- $(\mu_L/\mu_G) > 1000$ and mass velocities greater than 100 kg/m^{2}s (73,579 lb/h ft^2), the Chisholm (1973) correlation should be used.
- $(\mu_L/\mu_G) > 1000$ and mass velocities less than 100 kg/m^{2}s (73,579 lb/h ft^2), the Lockhart and Martinelli (1949) correlation should be used.
- For most fluids, $(\mu_L/\mu_G) < 1000$ and the Friedel correlation will be the preferred method for intube flow according to Whalley.

More recently, Tribbe and Müller-Steinhagen (2000) compared some of the leading two-phase frictional pressure drop correlations to a large database including the following combinations: air-oil, air-water, water-steam and several refrigerants. They found that statistically the method of Müller-Steinhagen and Heck (1986) gave the best and most reliable results. In another recent comparison, Ould Didi, Kattan and Thome (2002) compared the two-phase frictional pressure drop correlations described in the previous section to experimental pressure drops obtained in 10.92 and 12.00 mm (0.430 and 0.472 in.) internal diameter tubes of 3.013 m (9.885 ft) length for R-134a, R-123, R-402A, R-404A and R-502 over mass velocities from 100 to 500 kg/m^{2}s (73,579 to 367,896 lb/h ft^2) and vapor qualities from 0.04 to 0.99. Overall, they found the Grönnerud (1972) and the Müller-Steinhagen and Heck (1986) methods to be

equally best with the Friedel (1979) method the 3rd best. As an example, Figure 13.1 depicts a comparison of five of the above methods to some R-134a two-phase frictional pressure drop data.

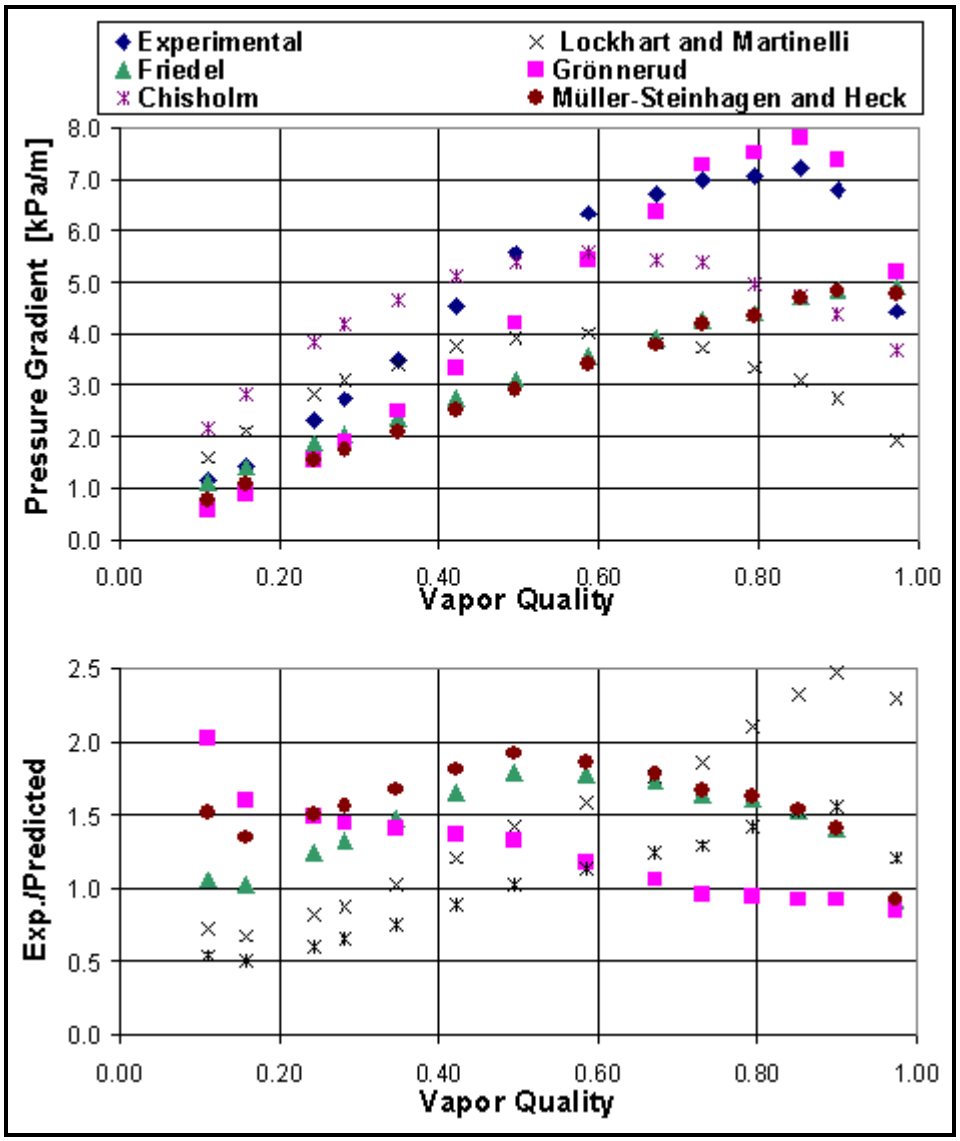

Figure 13.1. Five methods compared to R-134a evaporating in a 12.0 mm (0.472 in.) horizontal tube at 4.4 °C (40 °F) and 300 kg/m^{2}s (220740 lb/h ft^2).

In addition, Ould Didi, Kattan and Thome (2002) classified their data by flow pattern using the Kattan, Thome and Favrat (1998a) flow pattern map and thus obtained pressure drop databases for Annular flow, Intermittent flow and Stratified-Wavy flow. They found that the best method for annular flow was that of Müller-Steinhagen and Heck (1986), the best for Intermittent flow was that of Grönnerud (1972), and the best for Stratified-Wavy flow was that of Grönnerud (1972).

Two-phase friction pressure drop data of Moreno Quibén and Thome (2006a, 2006b) are compared in Figure 13.2 to two leading methods described above for R-22, R-410A and R-134a in 8.0 mm and 13.8 mm (0.315 and 0.543 in.) horizontal tubes, involving 1745 data points. Only about 40% of the data are captured within ±20% by the Grönnerud (1972) correlation whereas that of Müller-Steinhagen and Heck (1986) was the best of existing methods, but still not satisfactory with only 50% captured within ±20%.

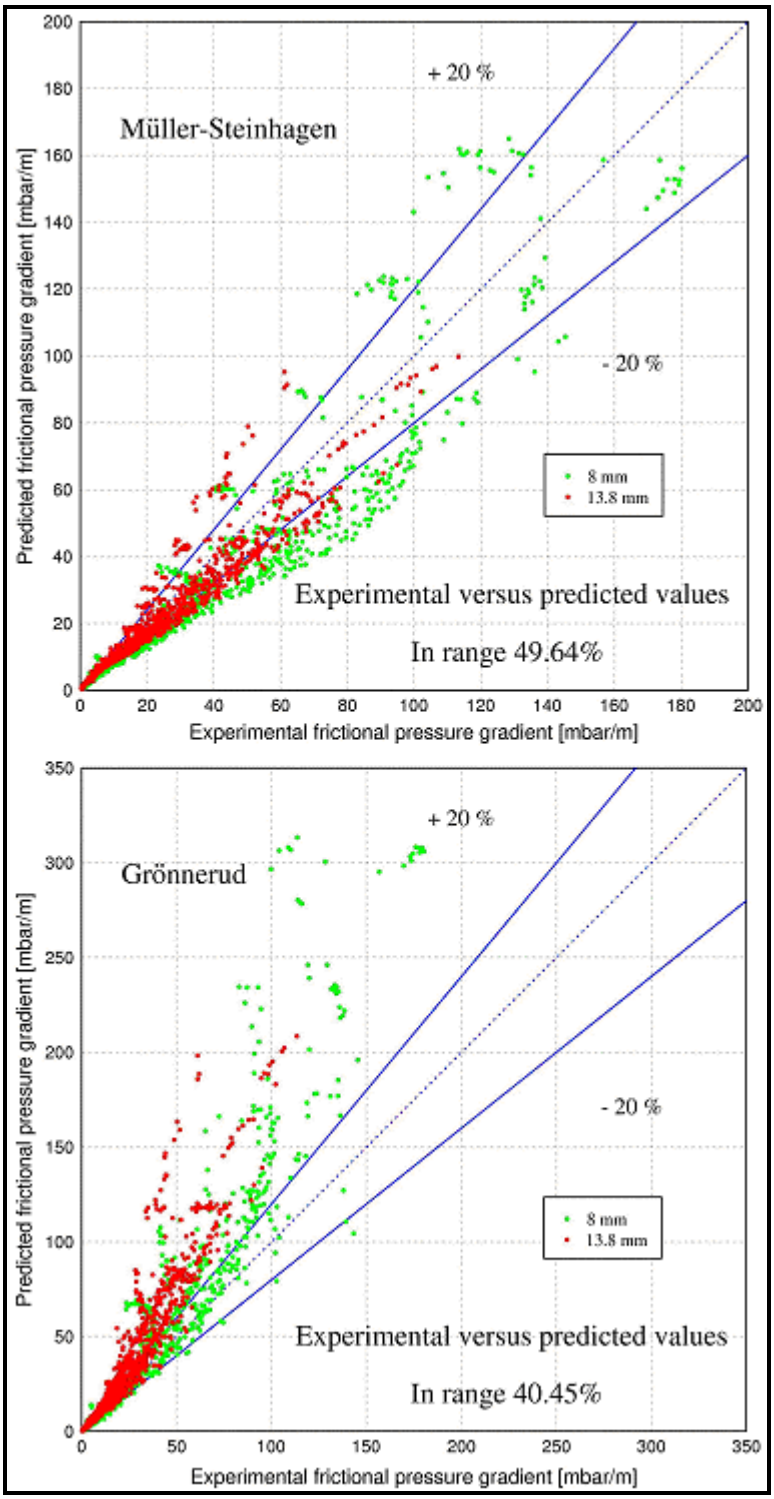

Figure 13.2. Two-phase friction pressure drop data of Moreno Quibén and Thome (2006a, 2006b) compared to two leading methods for R-22, R-410A and R-134a in 8.0 and 13.8 mm (0.315 and 0.543 in.) horizontal tubes.

In summary, even these "best" methods still have very large standard, mean and average deviations. Hence, the disagreement between measured pressure drops and predicted pressure drops using these methods can still easily be ±50% and sometimes more.

13.2.9 New flow pattern based two-phase pressure drop model

In an attempt to better capture the experimental trends and to improve the accuracy and reliability in the prediction of two-phase frictional pressure drops, Moreno Quibén and Thome (2006a, 2006b) proposed a new phenomenological two-phase frictional pressure drop model for horizontal tubes based on local flow patterns and interfacial wave effects for horizontal plain tubes. The complete description of the work is available in Moreno Quibén (2005). Their experimental study covered the following range of parameters: mass velocities from 70 to 700 kg/m^{2}s (51500 to 515000 lb/h ft^2), tube internal diameters of 8.0 mm and 13.8 mm (0.315 and 0.543 in.) and vapor qualities from 0.01 to 0.99, all at one saturation temperature of 5°C (41°F) for primarily R-22 and R-410A with a limited amount of data also for R-134a. Their two-phase frictional pressure drop database was obtained from both adiabatic and diabatic tests, the latter with heat fluxes from 6 to 57.5 kW/m^2 (1900 to 18230 Btu/h ft^2). They used the latest version of the Thome flow pattern map for adiabatic and evaporating flows in horizontal plain tubes proposed in Wojtan, Ursenbacher and Thome (2005a), to be described in an updated version of Chapter 12 in *Databook III*, to predict the local flow patterns in their pressure drop model. Below is a detailed description of their new flow pattern based frictional pressure drop model.

Simplified flow structures assumed for horizontal tubes. The same simplified flow structures assumed for evaporation inside horizontal tubes by Kattan, Thome and Favrat (1998c) and for condensation inside horizontal tubes by Thome, El Hajal and Cavallini (2003) were applied to the frictional pressure drop model, differing only in that the upper perimeter of the tube in a stratified type of condensing flow is wetted by film condensation rather than dry during evaporation (presently, the pressure drop data are for adiabatic and evaporating flows so the upper perimeter is assumed to be dry in stratified types of flow). The Moreno Quibén-Thome pressure drop model assumes three simplified geometries for describing annular flow, stratified-wavy flow and fully stratified-wavy flow as shown in Figure 13.3. For annular flow (bottom left), a uniform liquid film thickness of δ is assumed and the effects due to gravity are ignored. For fully stratified flow, the stratified geometry (upper left) is converted to an equivalent geometry (upper right) with the same angle of stratification and cross-sectional area occupied by the liquid, but with the liquid distributed as a truncated annular ring of uniform thickness δ as shown in the lower right diagram. In stratified-wavy flow (lower middle diagram), the interfacial waves are small and do not reach the top of the tube and hence the upper perimeter remains dry, and again it is assumed that the stratified-wavy liquid creates an annular truncated ring. Thus, the dry angle θ_{dry} varies between its maximum value of θ_{strat} at the threshold to fully stratified flow and its minimum value of zero at the threshold to annular flow.

Importantly, the three simple geometries shown above yield a smooth geometrical transition from one flow structure to another. A mist flow model with all the perimeter dry is used for that regime and prorations between these structures and the limits of all liquid flow at x = 0 and all vapor flow at x = 1 are applied to those boundaries. Figure 13.4 shows an example flow pattern map with the regimes considered by the present model, calculated using the Wojtan, Ursenbacher and Thome (2005a) map for the conditions noted. Below are the frictional pressure gradient prediction methods for individual flow regimes.

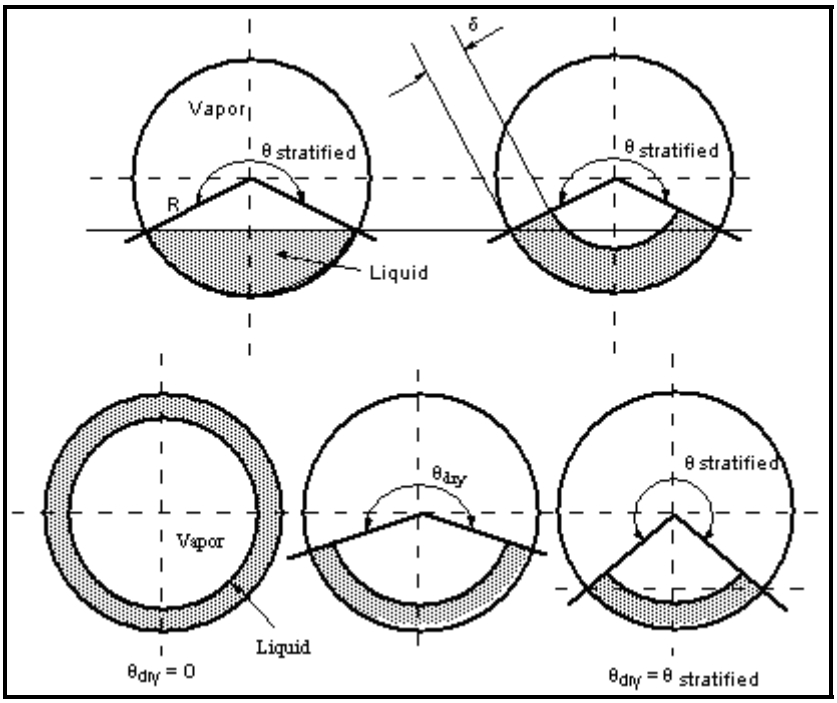

Figure 13.3. Simplified two-phase flow structures for pressure drop model. Lower left: annular flow structure, lower right: fully stratified flow structure equivalent to upper two figures, lower middle: stratified-wavy flow structure.

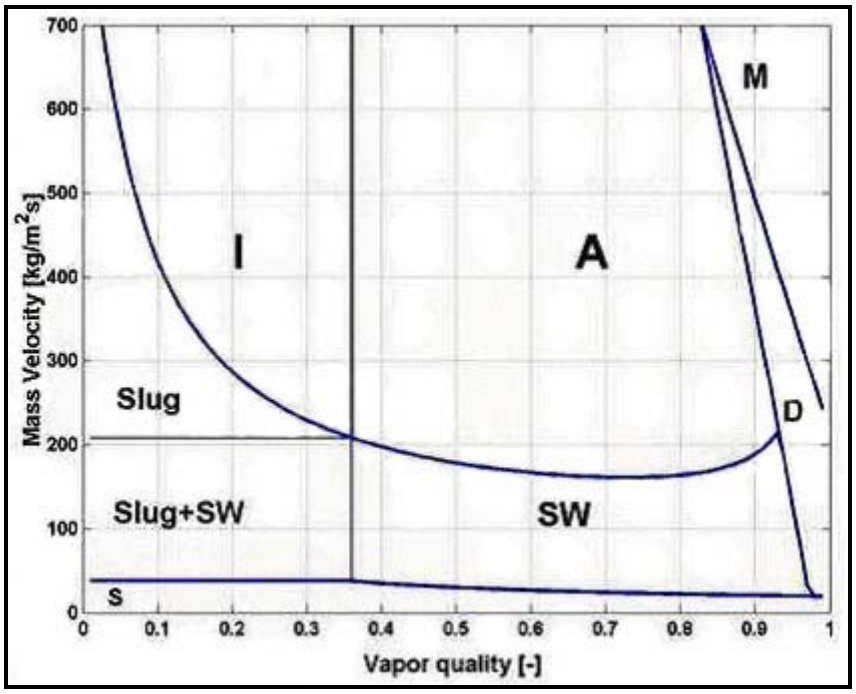

Figure 13.4. Flow pattern map for R-22 at Tsat = 5 oC (41°F) in the 13.84 mm (0.545 in.) test section with the void fractions evaluated using the mass velocity set to 300 kg/m^{2}s (220740 lb/h ft^2) and q = 7.5 kW/m^2 (2378 Btu/h ft^2).

Annular flow (A). The two-phase frictional pressure gradient in their model for annular flow is calculated with the following expression:

$$\left(\frac{dp}{dz}\right)_{annular} = 2(f_i)_{annular}\frac{\rho_G u_G^2}{d_i} \qquad [13.2.44]$$

Their interfacial film friction factor expression for annular flow is:

$$(f_i)_{annular} = 0.67\left[\frac{\delta}{d_i}\right]^{1.2}\left[\frac{(\rho_L-\rho_G)g\delta^2}{\sigma}\right]^{-0.4}\left[\frac{\mu_G}{\mu_L}\right]^{0.08} We_L^{-0.034} \qquad [13.2.45]$$

To the right of the equal sign in this expression, the first term scales the interfacial friction factor to the ratio of the film thickness to the tube diameter whilst the second term comes from a manipulation of the Helmholtz instability equation using δ as the scaling factor for the most dangerous wavelength for the formation of interfacial waves. This term is the same one used to implement the interfacial wave effect in the convective condensation heat transfer model by Thome, El Hajal and Thome (2003). The other two terms were used to bring in the viscosity ratio and surface tension effects. The empirical constant and exponents were obtained from analysis of only their annular flow pressure drop database. The liquid film thickness δ for a truncated annular ring as shown in Figure 13.3 is calculated from geometry to be:

$$\delta = \frac{d_i}{2} - \left[\left(\frac{d_i}{2}\right)^2 - \frac{(1-\varepsilon)\pi d_i^2}{2(2\pi-\theta_{dry})}\right]^{1/2} \qquad [13.2.46]$$

For annular flow $\theta_{dry} = 0$ and the cross-sectional void fraction ε is calculated using equation [13.2.4a] above. In implementing the calculation for δ, whenever $\varepsilon < 0.5$, δ is set equal to $d_i/2$ (the radius of the channel). The true average velocities of the two phases are calculated as:

$$u_G = \frac{\dot{m}_{total}\, x}{\rho_G \varepsilon} \qquad [13.2.47a]$$

$$u_L = \frac{\dot{m}_{total}(1-x)}{\rho_L(1-\varepsilon)} \qquad [13.2.47b]$$

In their method, the liquid Weber number is defined using the true average velocity of the liquid phase as:

$$We_L = \frac{\rho_L u_L^2 d_i}{\sigma} \qquad [13.2.48]$$

It should be noted that the above expressions can produce a maximum in the pressure gradient before reaching the transition to the dryout regime. This is because the annular film becomes very thin at high void fractions and hence its interfacial roughness diminishes accordingly, reducing friction like in the Moody diagram for roughened pipes.

Slug + intermittent flow (Slug + I). These two flow regimes were treated together since their experimental trends were noted to be similar. Rather than trying to capture their complex flow structures,

which would require methods to predict slug frequencies, slug and bubble lengths, etc., this regime was predicted using a proration between all liquid flow at x = 0 and annular flow at the intermittent-to-annular flow transition at x_{IA} using the void fraction ε as:

$$\left(\frac{dp}{dz}\right)_{slug+int\ ermittent} = \left(\frac{dp}{dz}\right)_L \left(1-\frac{\varepsilon}{\varepsilon_{IA}}\right)^{0.25} + \left(\frac{dp}{dz}\right)_{annular} \left(\frac{\varepsilon}{\varepsilon_{IA}}\right)^{0.25} \qquad [13.2.49]$$

The all liquid flow pressure gradient $(dp/dz)_L$ is calculated using expressions [13.2.6] to [13.2.8] with all the flow liquid and using liquid properties. In the above expression, $(dp/dz)_{annular}$ is the annular flow frictional pressure gradient from [13.2.44] using the actual vapor quality x of the slug or intermittent flow (not x_{IA}) in its evaluation with $\theta_{dry} = 0$ and also the actual value of x is used to calculate ε. At the limit of x = 0, this expression correctly reduces to that of an all liquid turbulent flow (or laminar flow but no such data were in their database) while at $x = x_{IA}$ it goes to the annular flow prediction without a jump in value at the transition. The value of ε_{IA} is obtained by evaluating [13.2.4a] with x set equal to x_{IA}. The proration exponent of 0.25 was determined statistically to be the best value to use for all such prorations in their method.

Stratified-wavy flow (SW). For this regime, the frictional pressure gradient is calculated from:

$$\left(\frac{dp}{dz}\right)_{stratified-wavy} = 2(f_i)_{stratified-wavy} \frac{\rho_G u_G^2}{d_i} \qquad [13.2.50]$$

The friction factor for stratified-wavy flow is obtained by a proration around the perimeter of the tube. The vapor phase friction factor is applied to the dry perimeter while that of annular flow is applied to the wetted perimeter as in the lower middle diagram in Figure 13.3, so that:

$$(f_i)_{stratified-wavy} = \theta^*_{dry} f_G + \left(1-\theta^*_{dry}\right)(f_i)_{annular} \qquad [13.2.51]$$

The friction factor for the lower wetted fraction of the perimeter of the tube $(f_i)_{annular}$ is calculated using [13.2.45] with the actual vapor quality in the calculation and using [13.2.46] to obtain the film thickness δ. The friction factor for the upper dry fraction of the perimeter of the tube f_G is calculated using [13.2.7] with vapor properties but here with the Reynolds number defined with respect to the true average vapor velocity in the cross-section of the tube occupied by the vapor:

$$Re_G = \frac{\dot{m}_{total}\, x\, d_i}{\mu_G \varepsilon} \qquad [13.2.52]$$

The upper dry fraction of the tube perimeter is obtained from its geometric definition:

$$\theta^*_{dry} = \frac{\theta_{dry}}{2\pi} \qquad [13.2.53]$$

The dry angle in a stratified-wavy flow is calculated based on the mass velocity of the flow using the following expression from Wojtan, Ursenbacher and Thome (2005b) and the transition boundary values of this flow regime from their flow pattern map:

$$\theta_{dry} = \left[\frac{\dot{m}_{wavy} - \dot{m}_{total}}{\dot{m}_{wavy} - \dot{m}_{s\ trat}}\right]^{0.61} \theta_{strat} \qquad [13.2.54]$$

Note that the wavy flow transition mass velocity is used in this calculation even when the upper boundary of the stratified-wavy flow regime on the flow pattern map becomes that of the dryout region; this is because if the dryout boundary were used, the value of θ_{dry} would incorrectly go to zero with increasing vapor quality. The stratified angle can be calculated explicitly from the following expression of Biberg (1999) from the value of the void fraction determined using [13.2.4a], avoiding use of its exact but iterative geometrical expression:

$$\theta_{strat} = 2\pi - 2\left\{\begin{array}{l}\pi(1-\varepsilon) + \left(\frac{3\pi}{2}\right)^{1/3}\left[1 - 2(1-\varepsilon) + (1-\varepsilon)^{1/3} - \varepsilon^{1/3}\right] \\ -\frac{1}{200}(1-\varepsilon)\varepsilon\left[1-2(1-\varepsilon)\right]\left[1+4\left((1-\varepsilon)^2+\varepsilon^2\right)\right]\end{array}\right\} \qquad [13.2.55]$$

Notice that this expression goes to the correct limits of $\varepsilon = 0$ at $x = 0$ and $\varepsilon = 1$ at $x = 1$.

Slug + stratified-wavy flow (Slug + SW). Referring to the flow pattern map shown in Figure 13.4, it is seen that this flow regime is bounded by slug flow at the top, fully stratified flow at the bottom, stratified-wavy flow at the right and all liquid flow at the left. Hence, these transition boundaries were taken into account when they proposed the frictional pressure drop method for this regime without any jumps in its values at these boundaries. Furthermore, in this regime Wojtan, Ursenbacher and Thome (2003) observed a cyclic behaviour of the flow, alternating between low amplitude waves that did not reach the top of the tube and slug flow with its large amplitude waves washing the top of the tube perimeter. The following expression was found by Moreno Quibén and Thome to reflect these observations and limits:

$$\left(\frac{dp}{dz}\right)_{slug+SW} = \left(\frac{dp}{dz}\right)_L \left(1 - \frac{\varepsilon}{\varepsilon_{IA}}\right)^{0.25} + \left(\frac{dp}{dz}\right)_{stratified-wavy} \left(\frac{\varepsilon}{\varepsilon_{IA}}\right)^{0.25} \qquad [13.2.56]$$

The values of $(dp/dz)_L$ and ε_{IA} are evaluated as explained already above while $(dp/dz)_{stratified\text{-}wavy}$ is the stratified-wavy flow frictional pressure gradient from [13.2.50] using the actual vapor quality of flow in its calculation and that of ε. Referring again to Figure 13.4, θ_{dry} is obtained from [13.2.54] by using the horizontal upper and lower transition boundaries of this regime, whose respective mass velocity values are those at x_{IA}. The value of δ is obtained using [13.2.46]. It should be pointed that when $\varepsilon < 0.5$, the liquid occupies more than one-half of the cross-section of the tube. Hence, the convention used in their method is that whenever $\varepsilon < 0.5$, δ is set equal to $d_i/2$. This convention still brings their method to the correct pressure gradient for all liquid flow at $x = 0$ because of the proration.

Mist flow (M). The mist flow regime is characterized by all the liquid entrained in the continuous vapor phase as minute droplets. The droplets travel at nearly the same velocity as the vapor and hence the homogeneous model given by [13.1.4] is used to determine the homogeneous void fraction ε_H. For homogeneous flows as explained earlier, the flow is assumed to be one fluid possessing mean fluid properties. The frictional pressure gradient of a mist flow is obtained from manipulation of [13.1.6] to be:

$$\left(\frac{dp}{dz}\right)_{mist} = \frac{2(f_i)_{mist}\dot{m}_{total}^2}{d_i \rho_H} \qquad [13.2.57]$$

The expressions [13.1.7], [13.1.8] and [13.1.9] presented in Section 13.1 are then used to calculate the mist flow friction factor. At the limit of x = 1 where ε = 1, this expression goes to the limit of an all vapor flow frictional pressure gradient. While this may at first appear to be a satisfactory bound, in reality the entrained droplets in a mist flow are typically not yet all evaporated and the pressure drops measured at x = 1 are usually still larger than would otherwise be expected. This aspect has not yet been taken into account in the Moreno Quibén-Thome flow pattern based pressure drop model.

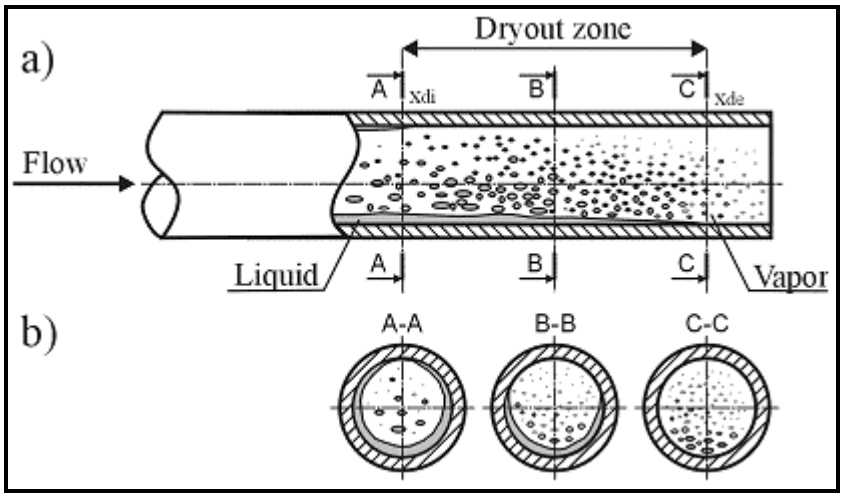

Figure 13.5. Schematic diagram of transition from annular flow to mist flow through the dryout regime: (a) side view, (b) cross-sectional view.

Dryout flow (D). Figure 13.5 depicts a schematic diagram of the transition from annular flow to mist flow at low to medium mass velocities, passing through the dryout regime. Since the annular film is thinner at the top than the bottom of the tube, the upper film becomes entrained as droplets in the vapor core first, leaving the lower perimeter still wet. Referring to Figure 13.4, this regime is bounded at the left by the annular and stratified-wavy flow regimes and at the right by the mist flow regime. At high mass velocities, the left and right transition lines of the dryout regime meet and form one line, and hence the dryout regime at that point disappears. This disappearance seems to reflect the actual process because at high mass velocities the thickness of the annular film at the top and bottom of the tube become identical as gravity effects have become negligible and hence entrainment should then happen simultaneously around the entire perimeter. For such situations, the frictional pressure drop gradient *jumps* from the annular flow value to the mist flow value, again probably reflecting the actual process (no data at these conditions were obtained in their experimental study to verify this, however). When the dryout regime does exist, the following linear interpolation was used to capture the variation in frictional pressure gradient across this regime without introducing any jump in the value:

$$\left(\frac{dp}{dz}\right)_{dryout} = \left(\frac{dp}{dz}\right)_{x=x_{di}} - \frac{x - x_{di}}{x_{de} - x_{di}}\left[\left(\frac{dp}{dz}\right)_{x=x_{di}} - \left(\frac{dp}{dz}\right)_{x=x_{de}}\right] \qquad [13.2.58]$$

In this expression, x_{di} is the inception quality of dryout at the top of the tube and x_{de} is the dryout completion quality at the bottom of the tube. The value of frictional pressure gradient at $x=x_{di}$ is obtained using either [13.2.44] or [13.2.50] for annular and stratified-wavy flows, respectively, evaluated for x set equal to x_{di}. The value of mist flow frictional pressure gradient at $x=x_{de}$ is calculated using [13.2.57] with

x set equal to x_{de}. Wojtan, Ursenbacher and Thome (2005a) gave the following prediction methods for x_{di} and x_{de}:

$$x_{di} = 0.58 \exp\left[0.52 - 0.000021 We_G^{0.96} Fr_G^{-0.02} \left(\frac{\rho_G}{\rho_L} \right)^{-0.08} \right] \quad [13.2.59]$$

$$x_{de} = 0.61 \exp\left[0.57 - 0.0000265 We_G^{0.94} Fr_G^{-0.02} \left(\frac{\rho_G}{\rho_L} \right)^{-0.08} \right] \quad [13.2.60]$$

In these expressions, the Weber and Froude numbers are defined as:

$$We_G = \frac{\dot{m}_{total}^2 d_i}{\rho_G \sigma} \quad [13.2.61]$$

$$Fr_G = \frac{\dot{m}_{total}^2}{\rho_G (\rho_L - \rho_G) g d_i} \quad [13.2.62]$$

At high mass velocities, the transition line of x_{de} intersects with that of x_{di} and above this intersection the value of x_{di} is tentatively used as the direct transition between annular and mist flow. At very low mass velocities, the lower bound of this flow regime is fully stratified flow, the latter which extends from x = 0 all the way to x = 1.0. Implementing the expression for x_{de} one will also find that when decreasing the mass velocity one reaches a value of x_{de} = 1.0, which is the maximum possible value of x_{de} even when [13.2.60] yields values larger than 1.0.

Stratified flow (S). Although no fully stratified two-phase pressure drop data were obtained in the study of Moreno Quibén and Thome (2006a, 2006b), a logical extension of their above model to stratified flows without imposing any jumps at the stratified flow transition boundary was proposed. If $x_{IA} \le x \le x_{di}$, then the friction factor for stratified flow is calculated as:

$$(f_i)_{stratified} = \theta^*_{strat} f_G + (1 - \theta^*_{strat})(f_i)_{annular} \quad [13.2.63]$$

Similar to the method for stratified-wavy flow, the single-phase vapor friction factor is calculated with [13.2.7] in the same manner as noted above and the friction factor for the lower wetted fraction of the perimeter of the tube $(f_i)_{annular}$ is calculated using [13.2.45] with the actual vapor quality in the calculation and using [13.2.46] to obtain the film thickness δ while the value of θ_{dry} becomes that of θ_{strat}, such that:

$$\theta^*_{strat} = \frac{\theta_{strat}}{2\pi} \quad [13.2.64]$$

The frictional pressure gradient for stratified flow then is obtainable from:

$$\left(\frac{dp}{dz} \right)_{stratified(x \ge x_{IA})} = 2 (f_i)_{stratified} \frac{\rho_G u_G^2}{d_i} \quad [13.2.65]$$

If $0 \le x < x_{IA}$, then the frictional pressure gradient for stratified flow is given by the following proration between all liquid flow and [13.2.65] evaluated with the actual vapor quality:

$$\left(\frac{dp}{dz}\right)_{\text{stratified}\,(x<x_{IA})} = \left(\frac{dp}{dz}\right)_{L}\left(1-\frac{\varepsilon}{\varepsilon_{IA}}\right)^{0.25} + \left(\frac{dp}{dz}\right)_{\text{stratified}\,(x\ge x_{IA})}\left(\frac{\varepsilon}{\varepsilon_{IA}}\right)^{0.25} \qquad [13.2.66]$$

As can be observed in Figure 13.4, the stratified regime extends all the way to x = 1.0 and the lower bound of the transition line for x_{di} stops at the stratified flow boundary. For the small range where the vapor quality in a stratified flow is larger than x_{di}, the frictional pressure gradient could experience a jump at the stratified flow to dryout boundary when changing the mass velocity. Since this is not significant in practice, this minor jump has been ignored in their method. The problem can be resolved with a small modification to the flow pattern map by allowing the x_{di} transition line to go all the way to zero mass velocity, at which point $x_{di} = 0.976$. Then the expression [13.2.58] would be applicable to this small area and the limit of all vapor flow at x = 1 would still be respected.

Bubbly flow (B). A prediction method for bubbly flows was not addressed in their pressure drop model as they had no test data in this regime. Bubbly flows tend to occur in horizontal tubes at very high mass velocities beyond the range of industrial interest.

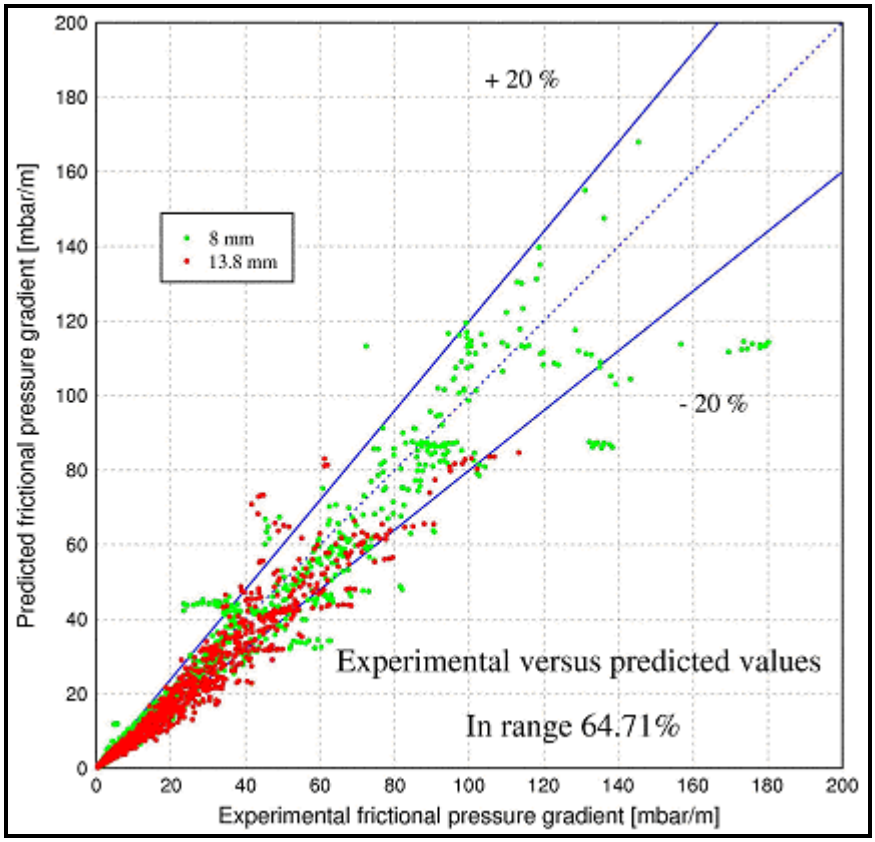

Figure 13.6. Two-phase frictional pressure drop data of Moreno Quibén and Thome (2006a, 2006b) compared to their new flow pattern based method for R-22, R-410A and R-134a in 8.0 and 13.8 mm (0.315 and 0.543 in.) horizontal tubes.

Comparison of the new flow regime model to their database. Figure 13.6 shows the two-phase frictional pressure drop data of Moreno Quibén and Thome (2006a, 2006b) compared to their new flow pattern based method for R-22, R-410A and R-134a in 8.0 mm and 13.8 mm (0.315 and 0.543 in.) horizontal tubes. A statistical comparison of their new flow pattern based model versus the best three of the older models is shown in Table 13.2. As can be seen, the new flow pattern based model is able to predict more than 4 of every 5 data points within ±30% while also getting about 2 out of 3 within ±20%, which are both considerable improvements on the older competing methods. As can be noted, the simpler to implement method of Müller-Steinhagen and Heck (1986) comes in second best here and in fact captures about 3 of every 4 data points within ±30%; it tends to not work well at high vapor qualities (typical of direct-expansion evaporator design conditions) and for stratified-wavy flows.

Table 13.2. Statistical comparison of data to four methods.

Data predicted within	±30%	±20%
Friedel (1979)	67.3%	51.8%
Grönnerud (1972)	46.2%	40.5%
Müller-Steinhagen and Heck (1986)	75.8%	49.6%
Moreno-Quibén and Thome (2006b)	82.3%	64.7%

Composite simulations of (i) the flow pattern map of Wojtan, Ursenbacher and Thome (2005a), (ii) the flow pattern based two-phase frictional pressure drop model of Moreno-Quibén and Thome (2006b), and (iii) the flow pattern based flow boiling model of Wojtan, Ursenbacher and Thome (2005b) for R-410A at 5°C (41°F) at two heat flux levels at a mass velocity of 300 kg/m^{2}s (220740 lb/h ft^2) are shown in Figure 13.7. Comparing the upper graph to the lower one, one can appreciate the effect of heat flux on the location of the boundaries of the dryout regime. Furthermore, one can note that the peak in the two-phase frictional pressure drop gradient does not necessarily coincide with the peak in the local flow boiling heat transfer coefficient, which was also noticed in their experimental results. The explanation for this is that the peak in the frictional pressure drop in an annular flow occurs either within the annular flow regime as the liquid film becomes very thin and reduces the interfacial surface roughness or when the onset of dryout at x_{di} occurs, which ever is reached first, whereas the heat transfer coefficient continues to increase until x_{di} is reached. Regarding the flow pattern based model, most of the points predicted with errors larger than 20-30% are those near flow pattern transition boundaries, particularly those at which a large change in trend occurs, such as at x_{di} and x_{de}. In this latter case, a map error of 2-3% in predicting the values of x_{di} and x_{de} or in the measurement of the vapor quality can lead to large errors because of the sharp change in slope of the pressure gradient in the dryout zone.

From a point of view of a recommendation, the new flow pattern based model is the most complete of those present in the literature, also capturing the trends in experimental data better than the older methods, but on the other hand it is more complex to implement and still requires more verification (and thus possible improvements) versus a broader range of fluids, pressures and tube sizes. So far, the individual phases have always been considered to be turbulent while in the future the database and model need to be expanded to cover laminar and transition regimes as well.

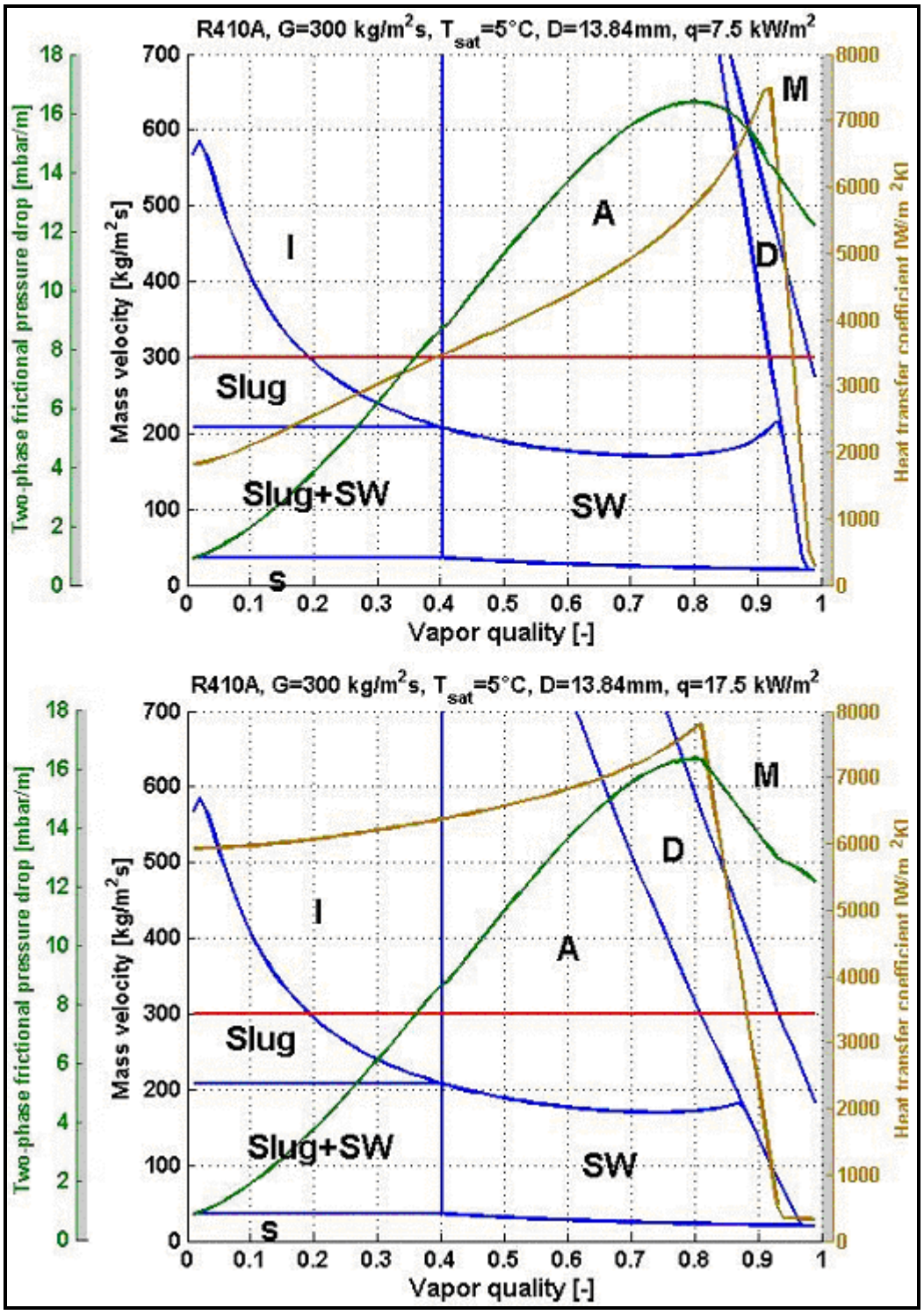

Figure 13.7.Composite simulations of (i) the flow pattern map of Wojtan, Ursenbacher and Thome (2005a), (ii) the flow pattern based two-phase frictional pressure drop model of Moreno-Quibén and Thome (2006b), and (iii) the flow pattern based flow boiling model of Wojtan, Ursenbacher and Thome (2005b) for R-410A at 5°C (41°F) at two heat fluxes levels and a mass velocity of 300 kg/m2s (220740 lb/h ft2).

13.2.10 Two-phase pressure drops in flattened plain tubes

Thome and Moreno Quibén (2004) completed an extensive experimental study on two-phase pressure drops inside horizontal flattened plain tubes. The tube samples they tested are shown in Figure 13.8 and the dimensions of the flattened tube geometries are shown in Figure 13.9 with internal heights of 2 and 3 mm (0.079 and 0.118 in.). The 13.8 mm (0.543 in.) flattened tubes had equivalent diameters of 8.60 and 7.17 mm (0.339 and 0.282 in.) and hydraulic diameters of 4.40 and 3.24 mm (0.173 and 0.128 in.), respectively, while the 8.0 mm (0.315 in.) flattened tubes had equivalent diameters of 6.25 and 5.30 mm (0.246 and 0.209 in.) and hydraulic diameters of 3.55 and 2.80 mm (0.140 and 0.110 in.), respectively. The hydraulic diameter is the traditional single-phase flow definition while an equivalent diameter is that of a round tube whose cross-sectional area is equal to that of the flattened tube. The latter definition seems to be more appropriate for two-phase flows since it keeps the mass velocities and velocity ratio of the two phases the same as in the flattened tube while a hydraulic diameter definition does not. In fact, they found that applying the equivalent diameter approach in their frictional prediction method yielded better results. The flattened tube samples were provided by Wolverine Tube, Inc. and were made by an extrusion process to obtain a more accurate and uniform shape than possible from simply flattening a tube in a press. The flattened tubes were tested with their flat sides oriented horizontally.

Figure 13.8. Photograph of round and flattened tubes.

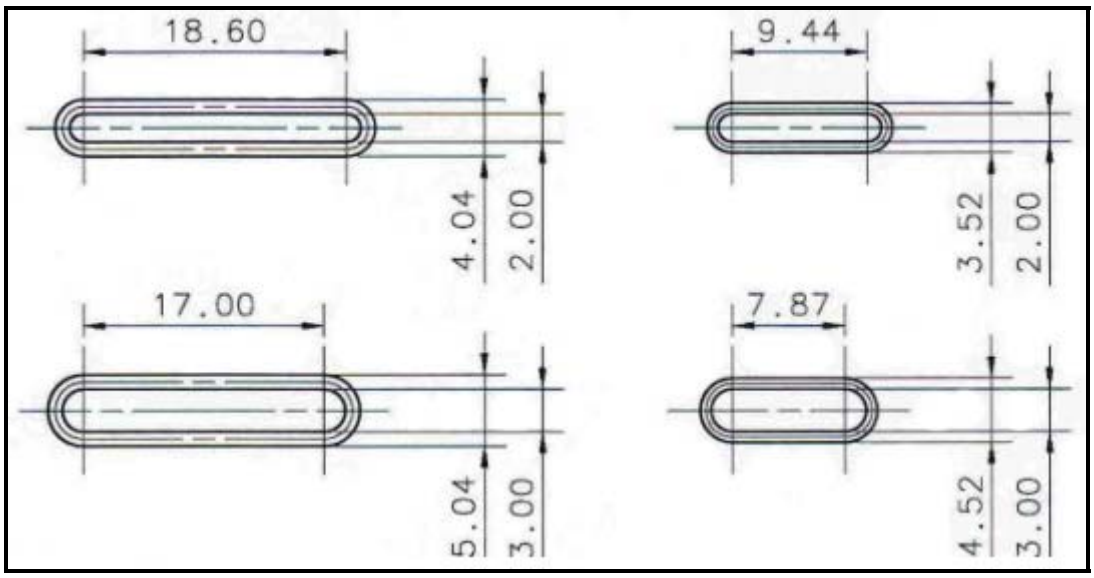

Figure 13.9. Dimensions of the flattened tubes studied.

Figure 13.10 depicts some of their two-phase pressure drop data measured for the larger size tube samples for R-22 and R-410A. As can be noticed, the pressure drop penalty of the flattened tubes at the same mass velocity as the round tube can be as high as seven! Thus, careful thermal design to find a balance between heat transfer and pressure drop is required for applying flattened tubes to reduce refrigerant charge in such evaporators.

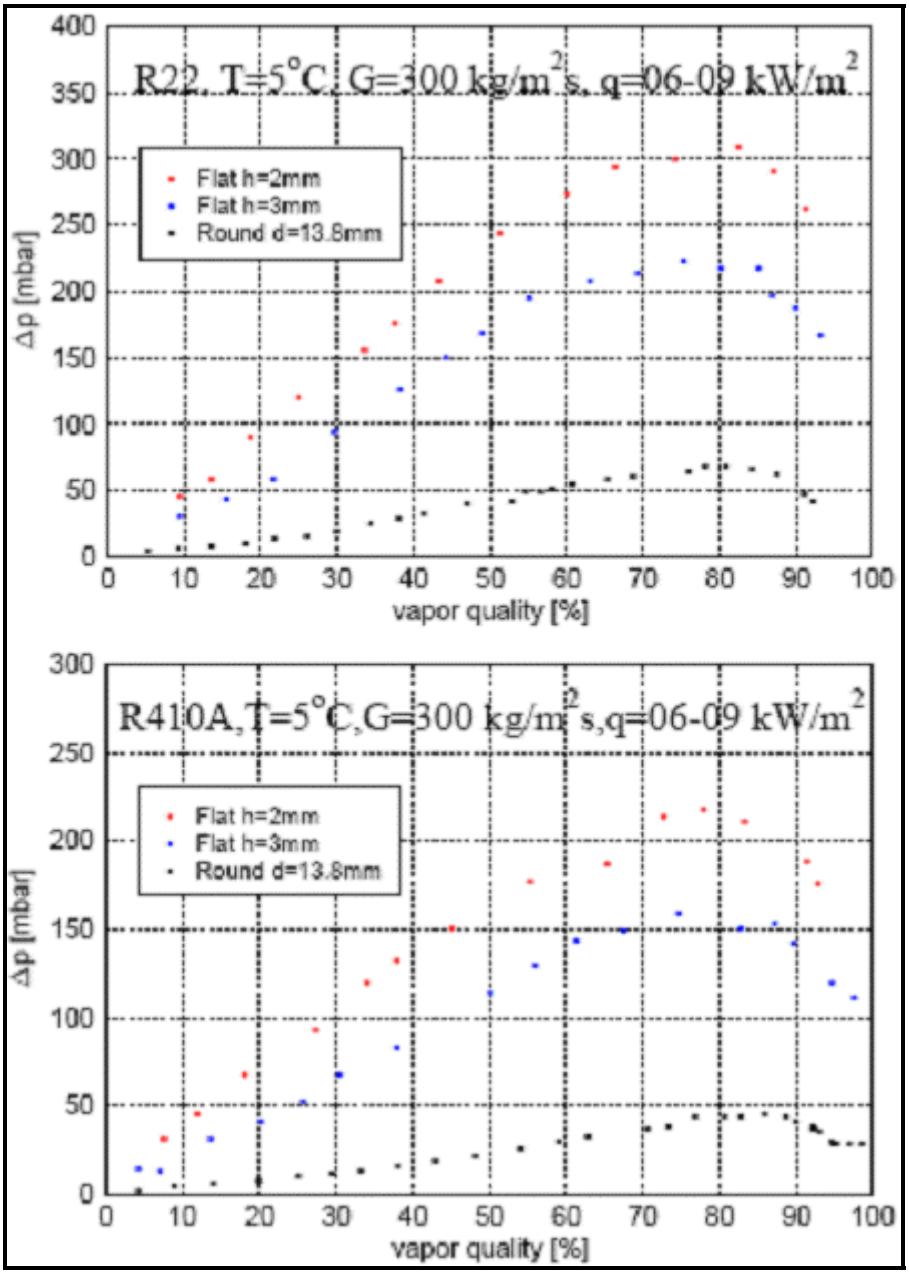

Figure 13.10. Flattened tube pressure drop data for round 13.8 mm (0.543 in.) tube and flattened versions with heights of 2 and 3 mm (0. 079 and 0.118 in.). Top: Results for R-22; bottom: Results for R-410A.

To predict the two-phase frictional pressure drops in flattened tubes, Thome and Moreno Quibén (2004) modified the method of Grönnerud (1972) presented above. The modified expression became:

$$\Delta p_{frict} = \Phi_{gd} \Delta p_L F_{round} F_{flat} \qquad [13.2.67]$$

His two-phase multiplier given by [13.2.23] and the calculation of Δp_L remain the same as in the original method except that the equivalent diameter is used in place of d_i. The mass velocity is based on the actual cross-sectional area of the flattened tube. To correct the Grönnerud method to better predict their round tube data over the entire range of vapor qualities, they applied the correction factor F_{round} as:

$$F_{round} = 1.21 - 0.63x \qquad [13.2.68]$$

To then correct the method to fit the flattened tube data, one further correction factor F_{flat} was applied:

$$F_{flat} = 3.2 - 1.42x \qquad [13.2.69]$$

Figure 13.11 shows a comparison of the predicted values to those measured. The flattened tube method captured most of their 359 data points within ±30% error and also followed the trends in the experimental data. Their tests covered R-22 and R-410A at 5°C (41°F) over nearly the entire vapor quality range for mass velocities from 150 to 500 kg/m^{2}s (110400 to 367900 lb/h ft^2).

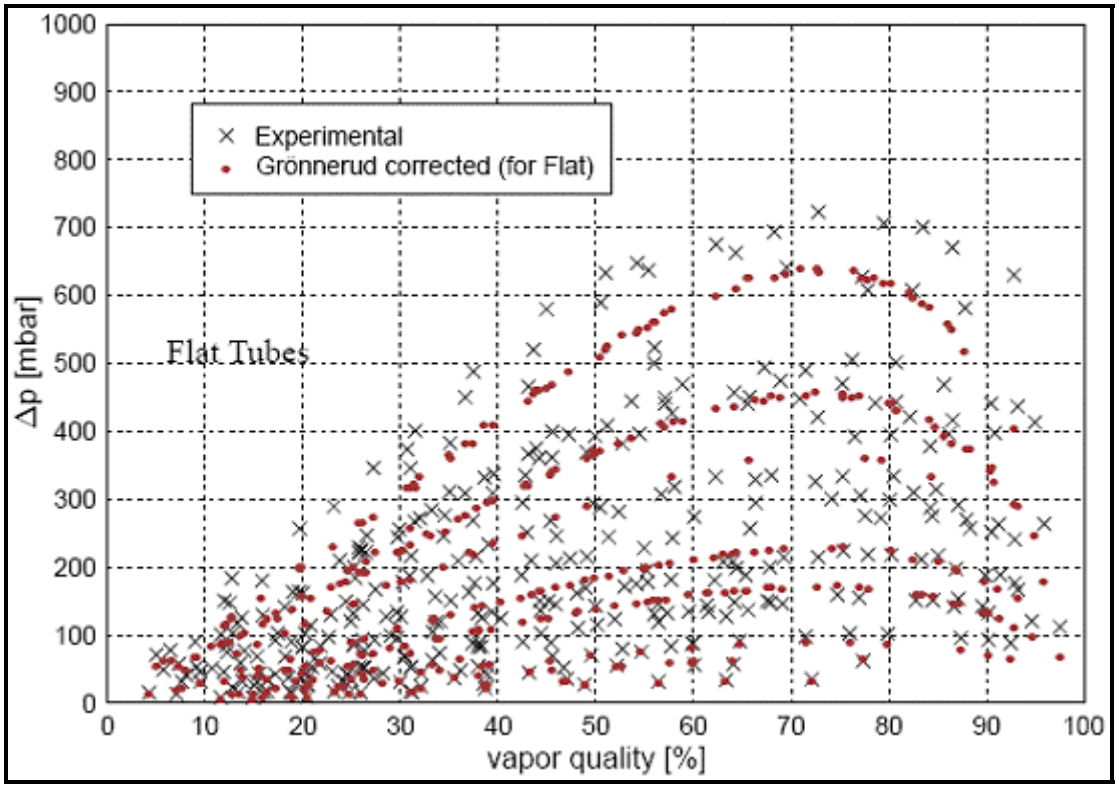

Figure 13.11. Comparison of predictions to measurements for flattened tube data.

13.3 Two-Phase Pressure Drops in Microfin Tubes

Thors and Bogart (1994) measured two-phase pressure drops for a 3.66 m (12 ft) long horizontal test sections of 9.53 mm (3/8 in.) and 15.9 mm (5/8 in.) diameter tubes for several microfin tubes in

comparison to plain bore tubes for R-22 at a saturation temperature of 1.67°C (35°F) for evaporation from an inlet vapor quality of 10% to an outlet vapor quality of 80%. Figure 13.12 depicts their comparison of two-phase pressure drops for the smaller tubes: plain tube of 8.72 mm (0.343 in.) internal diameter, microfin tube of 8.87 mm (0.349 in.) internal diameter with 60 fins of 18° helix angle and 0.203 mm height (0.008 in.) and microfin tube of 8.87 mm (0.349 in.) internal diameter with 72 fins of 0° helix angle and 0.203 mm height (0.008 in.). As can be noted, the pressure drops for the longitudinal micron fin tube are identical to those of the plain tube, i.e. no pressure drop penalty, while those of the 18° microfin tube are only marginally higher at the higher mass velocities (by about 10-20%).

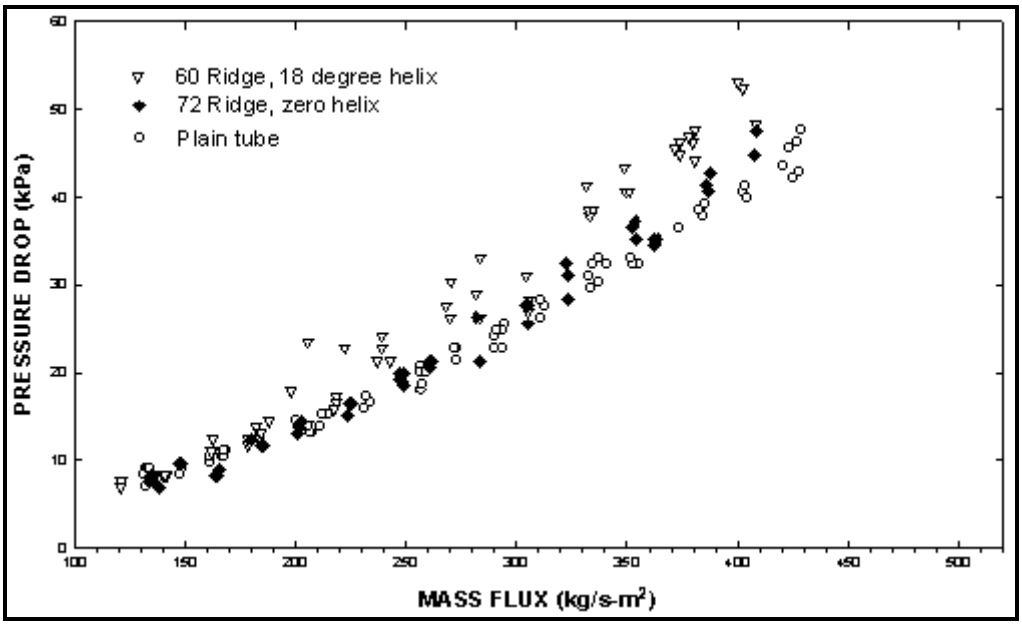

Figure 13.12. Thors and Bogart (1994) comparison of two-phase pressure drops for R-22 in 9.53 mm (3/8 in.) tubes.

Similarly, in Figure 13.13 their comparable results for the large tube size are shown. The tests were run for the following tubes: plain tube of 14.86 mm (0.585 in.) internal diameter, microfin tube of 14.86 mm (0.585 in.) internal diameter with 60 fins of 27° helix angle and 0.305 mm height (0.012 in.), microfin tube of 14.86 mm (0.585 in.) internal diameter with 75 fins of 23° helix angle and 0.305 mm height (0.012 in.) and corrugated tube of 14.10 mm (0.555 in.) internal diameter with one start giving a helix angle of 78° and corrugation depth of 1.041 mm (0.041 in.). Here, the microfin tubes have the same pressure drop as the plain tube at low mass velocities while they are up to 50% higher at the highest mass velocity. The corrugated tube also begins at the low mass velocity with the same pressure drop as the other tubes but then its pressure drop increases rapidly up to 200% higher than that of the plain tube and up to 100% higher than the microfin tubes.

In similar tests, Muzzio, Niro and Arosio (1998) presented a comparison of two-phase pressure drops for a variety of microfin tubes, arriving at similar conclusions to those above, i.e. microfin tubes have two-phase pressure drops similar or slightly higher than those of plain bore tubes. Numerous other studies on two-phase pressure drops for microfin tubes are in the literature, such as those of Schlager, Pate and Bergles (1990) for R-22, Chamra, Webb and Randlett (1996) for R-22, Nidegger, Thome and Favrat (1997) for R-134a and Zürcher, Thome and Favrat (1998b) for R-407C.

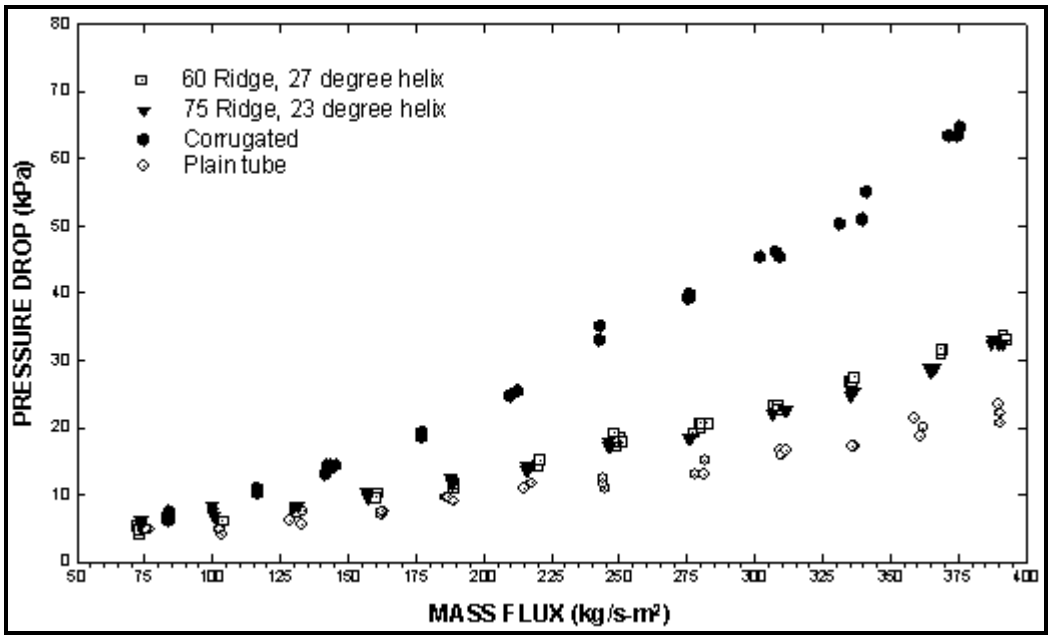

Figure 13.13. Thors and Bogart (1994) comparison of two-phase pressure drops for R-22 in 15.88 (5/8 in.) tubes.

Yashar et al. (2001) made comprehensive measurements for void fractions during evaporation and condensation in microfin tubes using the quick closing valve technique, which had an uncertainty of about 10%, which is quite large considering that two-phase pressure drops are particularly sensitive to the local void fraction. They correlated their data with the following method applicable to plain tubes and microfin tubes under evaporating and condensing conditions based on tests with R-134a and R-410a:

$$\varepsilon = \left(1 + \frac{1}{Ft} + X_{tt}\right)^{-0.321} \qquad [13.3.1]$$

where the Froude rate Ft is given as

$$Ft = \left(\frac{\dot{m}_{total}^2 x^3}{(1-x)\rho_G^2 g d_i}\right)^{0.5} \qquad [13.3.2]$$

The tube diameter d_i is that of the plain tube or that at the root of the fins of microfin tubes. The Martinelli parameter X_{tt} is given by Eq. 13.2.21. This method combines the effects of two important parameters: the Martinelli parameter, which is essentially a ratio of viscous drag effects to the vapor kinetic energy and the Froude rate, which is a ratio of the vapor kinetic energy to gravitational drag effects. This method, however, sometimes erroneously predicts void fractions larger than the homogeneous void fraction.

13.4 Two-Phase Pressure Drops in Corrugated Tubes

For two-phase flows in corrugated tubes, the two-phase pressure drops are typically much larger than those of plain tubes and microfin tubes. For example, Figure 13.13 depicted some experimental results of Bogart and Thors (1994) for R-22 compared to a plain tube and two microfin tubes. Withers and Habdas (1974) have presented an earlier experimental study on a corrugated tube for R-12. No general method is

available for predicting two-phase pressure drops in corrugated tubes. There are numerous tube diameters, corrugation depths and corrugation pitches among the tubes commercially available and there has apparently not been a systematic study to develop such a method.

13.5 Two-Phase Pressure Drops for Twisted Tape Inserts in Plain Tubes

A twisted tape insert is a metal strip that is twisted into a helix before its insertion into a plain tube. In order to install the twisted tape, its diameter must be slightly less than that of the tube, accounting for the normal manufacturing tolerance of tube wall thickness and roundness. Hence, twisted tapes are in rather poor contact with the tube wall. In fact, a large two-phase pressure drop may drive the insert out of the tube if it is not firmly fixed at the entrance.

For two-phase flows in tubes with twisted tape inserts, the two-phase pressure drops are typically much larger than those of plain tubes and microfin tubes and similar to those of corrugated tubes. No general method is available for predicting two-phase pressure drops in tubes with twisted tape inserts. As a rough approximation, the hydraulic diameter of one of the two flow channels inside the tube, which is bisected by the tape, can be used in one of the plain tube two-phase frictional pressure drop correlations, assuming one-half of the flow goes through this channel. This typically results in two-phase pressure drops twice as large as in the same tube without the tape.

13.6 Two-Phase Pressure Drops in Shell-side Flows

13.6.1 Plain tube bundles

The following approach is probably the best currently available. The total pressure drop Δp_{total} of a two-phase fluid flowing in cross-flow over a tube bundle is the sum of the static pressure drop (elevation head) Δp_{static}, the momentum pressure drop (acceleration) Δp_{mom}, and the frictional pressure drop Δp_{frict}:

$$\Delta p_{total} = \Delta p_{static} + \Delta p_{mom} + \Delta p_{frict} \qquad [13.6.1]$$

For shell-side flows, there is little known about the void fraction and since the bubbles formed would seem to have a velocity similar to that to the liquid-phase in this well-mixed type of flow, the static pressure drop is recommended to be determined using the homogeneous void fraction as:

$$\Delta p_{static} = \rho_H \, g \, H \sin \theta \qquad [13.6.2]$$

where H is the vertical height and the homogeneous density ρ_H is

$$\rho_H = \rho_L \, (1 - \varepsilon_H) + \rho_G \, \varepsilon_H \qquad [13.6.3]$$

The liquid and gas (or vapor) densities are ρ_L and ρ_G, respectively. The homogeneous void fraction ε_H is

$$\varepsilon_H = \frac{1}{1 + \left(\frac{u_G}{u_L} \frac{(1-x)}{x} \frac{\rho_G}{\rho_L} \right)} \qquad [13.6.4]$$

where u_G/u_L is the velocity ratio, or slip ratio (S), and is equal to 1.0 for a homogeneous flow. The momentum pressure drop is also calculated with the homogeneous void fraction as:

$$\Delta p_{mom} = \dot{m}^2_{total} \left\{ \left[\frac{(1-x)^2}{\rho_L (1-\varepsilon_H)} + \frac{x^2}{\rho_G \varepsilon_H} \right]_{out} - \left[\frac{(1-x)^2}{\rho_L (1-\varepsilon_H)} + \frac{x^2}{\rho_G \varepsilon_H} \right]_{in} \right\} \qquad [13.6.5]$$

The momentum pressure drop results in a decrease in the pressure of the fluid when $x_{out} > x_{in}$ (evaporation) but a decrease in pressure when $x_{out} < x_{in}$ (condensation). Hence, in condensation a pressure recovery occurs; however, it is common to ignore the momentum recovery in condenser design and use it as a design safety factor.

For prediction of two-phase frictional pressure drops, the method of Ishihara, Palen and Taborek (1980) is recommended. Their correlation as it applies to crossflow over a tube bundle is as follows:

$$\Delta p_{frict} = \Phi^2_{Ltt} \Delta p_L \qquad [13.6.6]$$

or

$$\Delta p_{frict} = \Phi^2_{Gtt} \Delta p_G \qquad [13.6.7]$$

where

$$\Delta p_L = 4 f_L N \dot{m}^2_{max} (1-x)^2 (1/2\rho_L) \qquad [13.6.8]$$

$$\Delta p_G = 4 f_G N \dot{m}^2_{max} x^2 (1/2\rho_G) \qquad [13.6.9]$$

N is the number of rows crossed and f_L and f_G are single-phase friction factors for tube bundles, which can be taken from ideal tube bank correlations for the particular tube layout and Reynolds number (refer to an appropriate textbook or handbook). The maximum mass velocity of all the flow across the minimum bundle cross-section is used in the above expression, i.e. as is common for single-phase flows over tube bundles. For evaluation of these expressions, the liquid Reynolds number is calculated using the liquid fraction of the flow and the vapor Reynolds number using the vapor fraction of the flow; furthermore, [13.6.6] is used when $Re_L > 2000$ while [13.6.7] is utilized when Re_L is ≤ 2000. Their database covered values of $X_{tt} > 0.2$ and seems to work well when above this value. The liquid and vapor two-phase multipliers that go with these two expressions are

$$\Phi^2_{Ltt} = 1 + \frac{C}{X_{tt}} + \frac{1}{X^2_{tt}}, \qquad C = 8 \qquad [13.6.10]$$

$$\Phi^2_{Gtt} = 1 + CX_{tt} + X^2_{tt}, \qquad C = 8 \qquad [13.6.11]$$

The Martinelli parameter X_{tt} is that for both phases in turbulent, given by Eq. 3.2.21.

For flooded evaporators, the static head (Δp_{static}) typically dominates as low mass velocities. Hence, the influence of the void fraction is particularly significant on the value of Δp_{total}, especially at low vapor

quality. For other types of heat exchangers, such as TEAM E-shells with their segmental baffles, the prediction method is much more complex since the flow in the windows in longitudinal to the tubes. Modeling of two-phase flows in such configurations is beyond the scope of the present review.

The above method has been simulated for complete evaporation (100% evaporation from inlet to outlet) of R-134a at a saturation temperature of 4.4 °C (40°F) and a mass velocity of 16 kg/m^{2}s (11,773 lb/h ft^2) by Casciaro and Thome (2001b). Their results are shown in Figure 13.14. The total pressure drop is plotted as a function of vapor quality from inlet to outlet in a tube bundle, which was composed of 8 vertical staggered tube rows with a triangular pitch of 22.22 mm (0.875 in) for a tube external diameter of 19.05 mm (0.75 in.). The combined contributions of the momentum pressure drop (M.P.D.) and the frictional pressure drop (F.P.D.) are about 20% while the static head (S.P.D.) is the dominant one.

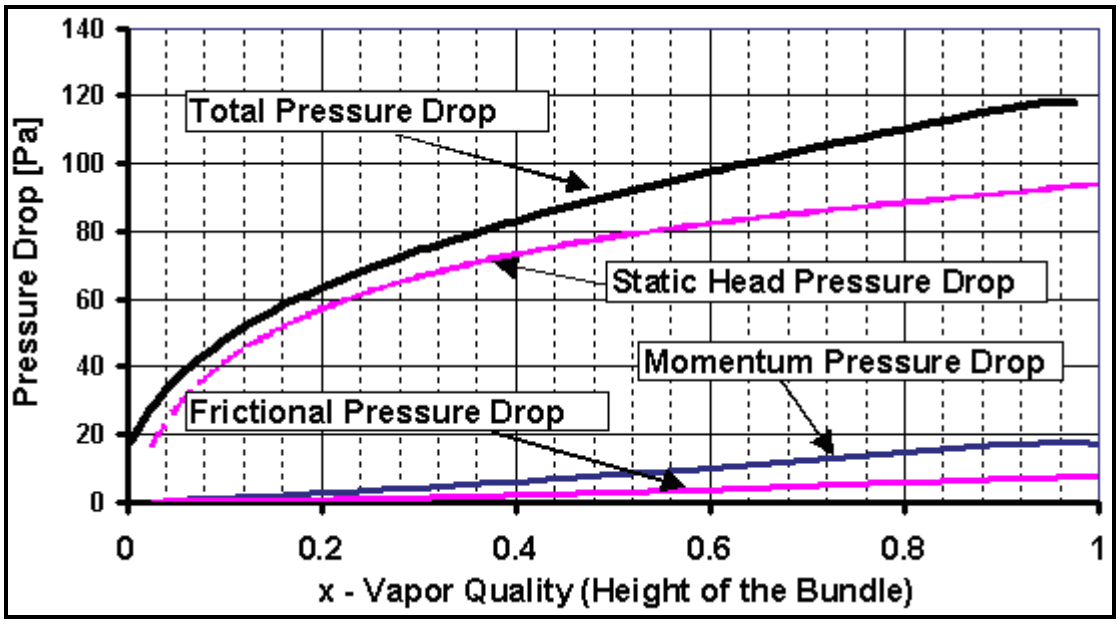

Figure 13.14. Pressure drop contributions in an evaporating shell-side flow at a constant mass velocity for R-134a [diagram from Casciaro and Thome (2001b) and reproduced from Int. J. HVAC&R Research].

For the same conditions as above, total pressure drops have been calculated for several mass velocities and are shown in Figure 13.15. In the range from 4 to 16 kg/m^{2}s (2,943 – 11,773 lb/h ft^2), there is not a big increase in the total pressure drop inside the tube bundle as the static pressure drop dominates. At higher mass velocities, the frictional pressure drop contribution becomes important.

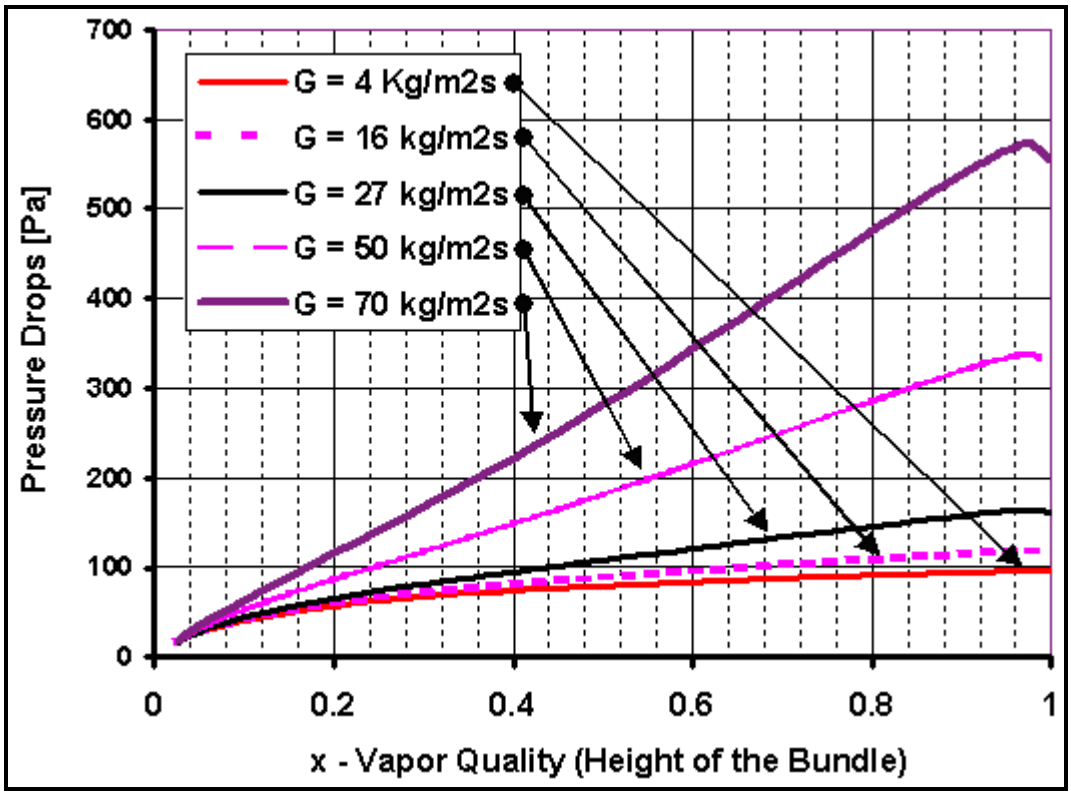

Figure 13.15. Total pressure drops as a function of shell-side mass velocity for R-134a [diagram from Casciaro and Thome (2001b) and reproduced from Int. J. HVAC&R Research].

13.6.2 Low finned tube and enhanced tube bundles

For prediction of two-phase pressure drops across a low finned tube bundle, the same method as recommended above is used except for the single-phase friction factors and the mass velocity. The mass velocity is calculated using the equivalent cross-flow area taking into account the area blocked by the fins. The single-phase frictional pressure drops are then calculated using the plain tube factors based on this mass velocity.

The Ishihara, Palen and Taborek (1980) method described above for *plain* tube bundles, in following the Martinelli approach, omits an explicit dependency of void fraction on the frictional pressure drop, which is likely to have an effect on the transport of momentum between and within the two phases since through the void fraction the ratio of the vapor to liquid velocity ratio is introduced. Furthermore, their database covered only conditions for $X_{tt} > 0.2$, which is above those typical in a flooded evaporator. Consequently, Consolini, Robinson and Thome (2006) have recently proposed a new tentative design method for *plain*, *low finned* and *enhanced* tube bundles. It covers the bundle, tube and test conditions described in Table 13.3, with liquid Reynolds numbers for R-134a ranging from about 240 to 3300, defined as:

$$Re_L = \frac{\dot{m}_{max} D}{\mu_L} \qquad [13.6.12]$$

For the vapor, the equivalent maximum Reynolds number reached about 70000. This means the liquid flow changes from laminar to transition flow within the database while the vapor flow will most likely

always be turbulent. The Reynolds numbers for R-410A and R-507A are approximately similar to those for R-134a. These liquid Reynolds numbers are much lower than those in the database of Ishihara, Palen and Taborek (1980), being representative of those confronted in flooded evaporator designs.

Table 13.3. Test conditions for method of Consolini, Robinson and Thome (2006).

Tube Type	Plain	Outside Diameter = 18.87 mm (0.743 in.)
	Low-Finned	Fin Tip Diameter = 18.92 mm (0.745 in.)
		Root Diameter = 15.88 mm (0.625 in.)
		Fin Height = 1.52 mm (0.060 in.)
		Fin Density = 1024 fins/m (26 fpi)
	Turbo-BII HP	Outside Diameter = 18.69 mm (0.736 in.)
		Root Diameter = 17.48 mm (0.688 in.)
Tube Pitch		22.22 mm (0.875 in.)
Tube Layout		Equilateral Triangle
Mass Velocity		3 to 42 kg/m^{2}s (2210-30920 lb/h ft^2)
Inlet Vapor Quality		0.08 to 0.50
Exit Vapor Quality		0.17 to 0.99
Saturation Pressure		R-134a: ~ 3.4 bar (49.8 psia)
		R-410A: ~ 9.2 bar (133.4 psia)
		R-507A: ~ 7.2 bar (104.4 psia)

In general, the two-phase frictional pressure drop is not the dominant component of the total pressure drop when the flow mass velocity is very low, but its importance increases with increasing mass velocity. Based on their analysis, Consolini, Robinson and Thome (2006) recommended using the Feenstra, Weaver and Judd (2000) void fraction method for tube bundles for calculating the static and momentum pressure drops, i.e. use ε from the Feenstra-Weaver-Judd method in [13.6.2], [3.6.3] and [13.6.5] instead of ε_H. This was the method they used to extract their frictional pressure drop and momentum pressure drop values from the measured total bundle pressure drops during boiling of the three refrigerants at the test conditions in Table 13.3. A description of the Feenstra, Weaver and Judd (2006) void fraction method is available in Chapter 17 in *Databook III*.

Consolini, Robinson and Thome (2006) proposed the following new two-phase frictional pressure drop method for low mass velocities:

$$\Delta p_{frict} = 4\lambda f N \dot{m}_{max}^2 (1/2\rho) \qquad [13.6.13]$$

In this expression, *f* refers to the fluid friction factor obtained using the appropriate single-phase tube bundle correlation, evaluated with the fluid Reynolds number defined as:

$$Re = \frac{\dot{m}_{max} D}{\mu} \qquad [13.6.14]$$

where the fluid density and viscosity are given by:

$$\rho = \rho_L (1-\varepsilon) + \rho_G \varepsilon \qquad [13.6.15]$$

$$\mu = \mu_L(1-\varepsilon) + \mu_G\varepsilon \qquad [13.6.16]$$

The local void fraction ε in the bundle is calculated with the Feenstra-Weaver-Judd method. In an approach that is somewhat similar to that proposed by Müller-Steinhagen and Heck (1986) for intube two-phase flow, the value of their two-phase friction factor multiplier λ is obtained from the expression:

$$\lambda = \Lambda + (1-\Lambda)(2x-1)^2 \qquad [13.6.17]$$

The value of λ goes to unity when the vapor quality goes to 0 and 1, i.e. the correct limits of all liquid and all vapor flow, respectively. Their experimental frictional pressure drops suggested a strong influence of the mass velocity on λ. Their correction factor Λ was thus obtained from:

$$\Lambda = \left(\frac{\dot{m}_{max}}{400}\right)^{-1.5} \qquad [13.6.18]$$

The local maximum mass velocity is input in kg/m^2s to non-dimensionalize Λ. This expression and method are valid over the conditions cited in Table 13.3. In their work, they utilized the single-phase friction factor correlations of Žukauskas and Ulinskas (1983).

To implement their frictional pressure drop method, one must: (i) evaluate the void fraction using the Feenstra-Weaver-Judd method, (ii) calculate the fluid density and viscosity using [13.6.15] and [13.6.16], (iii) calculate the fluid Reynolds number using [13.6.14]; (iv) use an appropriate tube cross-flow friction factor correlation for single-phase flow over tube bundles to calculate *f*, (v) obtain Λ and λ from [13.6.18] and [13.6.17], and (vi) calculate the two-phase frictional pressure drop from [13.6.13]. In the calculation of the maximum mass velocity in this method, the outside diameter of the plain tube or the diameter over the enhancement of an enhanced boiling tube is used. For the low finned tube bundle, the cross-sectional blockage diameter of the finned tube is used (which equals $D_{root} + 2te_f/s$ where D_{root} is the root diameter, t is the mean fin thickness, e_f is the fin height and s is the fin pitch).

Figure 13.16 depicts the predictions using their new two-phase frictional pressure drop method compared with their experimental database (showing pressure drop data from center of bundle, but similar results near the two ends) showing the ratio of the predicted total pressure drops divided by the corresponding experimental values. In predicting the total pressure drops, the static and momentum pressure drops were evaluated using the Feenstra, Weaver and Judd (2000) void fraction model, while the frictional contributions were obtained by their new method. This was implemented as a tube row by tube row stepwise calculation and then summing the incremental pressure drops. Most of the total pressure drops were predicted to within ±20% of their measured values; instead, extrapolating the Ishihara, Palen and Taborek (1980) frictional pressure drop method down to these low mass velocities, most of the data were under predicted by 50% or more. However, even though the Consolini-Robinson-Thome method was proposed in a general format and hence can be applied to other tube layouts, tube diameters, tube pitches, tube types, etc., it should still be considered as a preliminary method since it was developed only for one tube layout and tube pitch for a limited range of test conditions.

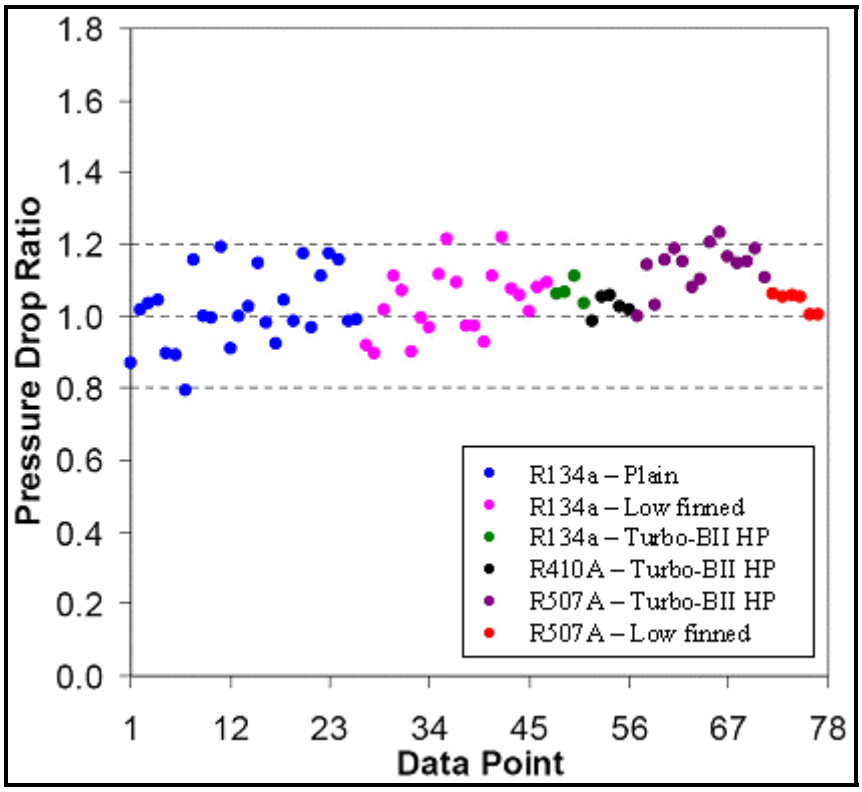

Figure 13.16. Comparison of total bundle pressure drops measured to predictions at central location along their test bundle.